

# Gravitational Landscapes: black holes with linear equations of state in asymptotically safe gravity

Ramin Hassannejad,<sup>1,\*</sup> Fatimah Shojai,<sup>1,†</sup> and Kazuharu Bamba<sup>2,‡</sup>

<sup>1</sup>*Department of Physics, University of Tehran, P.O. Box 14395-547, Tehran, Iran.*

<sup>2</sup>*Faculty of Symbiotic Systems Science, Fukushima University, Fukushima 960-1296, Japan.*

We study black holes with linear equation of state within the framework of asymptotically safe gravity. This study extends previous work on gravitational collapse in asymptotically safe gravity (that has been done for a dust fluid) by considering into account the pressure of stellar matter. We derive modified field equations containing the running gravitational coupling and the cosmological constant as functions of energy density. The interior space-time of collapsing star is modeled by the Friedmann-Lemaître-Robertson-Walker metric, while the exterior is described by a static spherically symmetric space-time. Different equations of state from ordinary matter to exotic phantom energy are considered to investigate their impact on black hole structure and horizon formation. Our results illustrate that asymptotically safe gravity can introduce non-singular black hole solutions under specific conditions. These results provide new insights into black hole physics and the avoidance of singularities within the asymptotically safe gravity framework.

## I. INTRODUCTION

For nearly half a century, black holes (BHs) have been a focal point of theoretical physics, serving as a complex intersection of gravity, quantum mechanics, and cosmology [1–14]. As objects formed by the gravitational collapse of massive stars [15–22], or were formed as a result of fluctuations in the early universe [23–25], BHs embody extreme physical conditions, where the spacetime curvature becomes so intense that even light cannot escape [1, 26]. According to general relativity, this collapse leads to the formation of a singularity, a region where physical quantities such as energy density and spacetime curvature diverge, signalling the failure of classical physics to describe the fabric of spacetime [1, 27, 28]. The breakdown of general relativity at singularities [29] requires a quantum theory of gravity, since quantum mechanical effects are expected to dominate in such regimes [13, 30–35]. Consequently, understanding the BH formation and the nature of the singularities is not only a central challenge in gravitational theory but also a crucial step towards a unified theory of quantum gravity [36–42]. Traditional models of BHs, based on Einstein’s field equations of general relativity, cannot fully deal with the problems posed by singularities. In classical general relativity, once the event horizon forms, the fate of the collapsing matter is to be crushed into an infinitely dense point [1]. Although this result is theoretically consistent within the framework of Einstein’s equations, it is physically unsatisfactory because it violates the known laws of physics, where infinities usually signal a limitation of the current theory [29, 43–45]. Moreover, the singularity problem illustrates that general relativity, while successful in describing

large-scale phenomena such as planetary motion and the expansion of the universe, requires modification at the quantum scale [13, 31, 46, 47]. The search for a quantum theory of gravity, that can resolve the issues of singularities and unify gravity with the other fundamental forces, has led to various proposals, including string theory [48], loop quantum gravity [49], and AS gravity [50, 51]. Of these, AS gravity is one of the most promising approaches to quantum gravity [52]. First introduced by Steven Weinberg in 1979 [53], AS gravity suggests that gravity becomes “safe” at high energies due to the presence of a non-trivial ultraviolet (UV) fixed point [33, 34, 54–56]. This fixed point ensures that the gravitational coupling constants, such as Newton’s constant, remain finite and well-behaved as the energy increases, thereby avoiding the divergences that typically plague quantum field theories at high energies [34, 35, 43]. The theory is rooted in the renormalization group approach [54, 57–63], which allows for the “running” of the coupling constants with energy, meaning that the strength of gravity and the cosmological constant are functions of the energy density of the system [35, 64]. Generally, the concept of asymptotic safety in gravity provides a potential solution to the singularity problem by suggesting that at extremely high densities, such as those found near the core of a BH, quantum gravitational effects modify the collapse dynamics and prevent the formation of a singularity [32, 65–67]. In addition to studies on BH solutions and massive objects in AS gravity, its cosmological implications have also been extensively investigated [68–72]. Notably, AS gravity has been applied to early cosmic inflation, as discussed in Ref. [73–78]. Other studies, such as AS gravity in the presence of a matter field, have been widely explored; see Ref. [79–84]. Although this theory has been widely studied, many open questions remain. One of the most fascinating aspects is its application to the physics of gravitational collapse, which we will delve into next.

---

\* [r.hassannejad@ut.ac.ir](mailto:r.hassannejad@ut.ac.ir)

† [fshojai@ut.ac.ir](mailto:fshojai@ut.ac.ir)

‡ [bamba@sss.fukushima-u.ac.jp](mailto:bamba@sss.fukushima-u.ac.jp)

In this paper, we extend the study of BHs within the framework of AS gravity by incorporating the effects of pressure through an equation of state (EOS) of the form  $p = w\rho$ , where  $p$  is the pressure,  $\rho$  the energy density, and  $w$  is a parameter that determines the type of matter or energy under consideration. The value of  $w$  influences the properties of the collapsing matter, and thus, the structure and behaviour of the resulting BH. A wide range of EOS parameters are considered in this study, from ordinary matter ( $w \geq 0$ ) to exotic forms of energy such as phantom energy ( $w < -1$ ) [85]. These different forms of matter significantly affect the nature of horizon formation, BH stability, and thermodynamic properties [86, 87]. The study of BHs with pressure is crucial because most astrophysical objects, such as stars, have significant internal pressure. Previous studies of BHs in AS gravity have focused primarily on the collapse of pressureless matter (dust) [64], but this simplification omits essential physical properties that play a critical role in real gravitational collapses [18–20]. The inclusion of pressure not only provides a more realistic model of BH formation but also allows a broader investigation of the effect of different EOS parameters on the dynamics of the collapse. For instance, while ordinary matter with  $w = 0$  (dust) leads to standard BH solutions, the inclusion of phantom energy ( $w < -1$ ) could lead to unusual BH structures, possibly avoiding singularities altogether [85]. This paper begins by deriving modified field equations that include the running gravitational coupling and the cosmological constant, both of which vary with the energy density of the collapsing matter. We model the interior of the collapsing star using the Friedmann-Lemaître-Robertson-Walker (FLRW) metric, a common choice in cosmology for describing homogeneous and isotropic spacetimes [88]. The exterior of the star, on the other hand, is described by a static, spherically symmetric solution, consistent with the traditional approach to modelling BH spacetimes. By analyzing a range of EOS parameters, we investigate how different types of matter affect BH structure, horizon formation, and the potential for non-singular solutions [32, 89]. Furthermore, we reformulate the field equations in terms of kinetic and potential energy, where the potential term provides deeper insight into the system's behavior. To this end, we first construct the Lagrangian for the FLRW spacetime and perform a Legendre transformation to obtain the corresponding Hamiltonian. This allows us to express the field equations in a form that explicitly separates kinetic and potential contributions. The dynamical stability of the system is then examined by analyzing the first and second derivatives of the potential function.

This paper is organized as follows: In Sec. II, we present the modified gravitational field equations incorporating the effects of AS gravity. Section III explores the dynamics of gravitational collapse with a linear EOS, including horizon formation and singularity

avoidance. Section IV analyzes the properties of the resulting BH solutions, emphasizing their stability and thermodynamics. Finally, in Sec. V, we summarize our findings and discuss the broader implications of our results for BH physics and AS gravity.

Throughout this paper, the signature of the metric tensor is assumed to be  $(-, +, +, +)$ . Unless explicitly specified, we use geometrized units, i.e.,  $c = \hbar = 1$ .

## II. THE GRAVITATIONAL FIELD EQUATION

It has been shown that a certain type of modified gravity theory tends to a de Sitter universe at high energy density [90]. This theory avoids the creation of singularities at high energy density limit. It is based on the idea that the gravitational coupling and the cosmological constant depend on the energy density ( $\epsilon$ ), represented as  $G(\epsilon)$  and  $\Lambda(\epsilon)$ , respectively. The field equation describing this theory is as follows

$$G^{\mu\nu} = 8\pi G(\epsilon)T^{\mu\nu} - \Lambda(\epsilon)g^{\mu\nu} = 8\pi T_e^{\mu\nu}, \quad (1)$$

where  $G^{\mu\nu}$  is the Einstein tensor, and  $T^{\mu\nu}$  is the perfect fluid energy-momentum tensor,

$$T^{\mu\nu} = (\epsilon + p)u^\mu u^\nu + pg^{\mu\nu}. \quad (2)$$

We can write the effective energy-momentum tensor in a way that resembles a perfect fluid

$$T_e^{\mu\nu} = (\rho_e + p_e)u^\mu u^\nu + p_e g^{\mu\nu}, \quad (3)$$

the functions  $G(\epsilon)$  and  $\Lambda(\epsilon)$  have the following properties: at high energy density limit,  $G(\epsilon)\epsilon$  approaches 0 and  $\Lambda(\epsilon)$  approaches  $\lambda$ , where  $\lambda$  is a constant. However, these conditions are not obligatory, but they must be considered in order to have a regular de Sitter space-time at high energy density  $\epsilon \gg 1$ . For a general case without the above conditions, the regularity of space-time is not required. In fact, this theory assumes that the fundamental coupling constants are dynamical and depend on the energy density. Their behavior at low and high energy densities alters the predictions of the field equations, and under some conditions it is possible to have regular space-time.

It was later shown (see Ref. [90]) that it is possible to derive the field equation (1) from a general Lagrangian which is expressed for a gravitational field and a hydrodynamic fluid as follows,

$$S = \frac{1}{16\pi G_0} \int \sqrt{-g} d^4x [\mathcal{R} + 2\chi(\epsilon)\mathcal{L}_\epsilon], \quad (4)$$

where  $\mathcal{L}_\epsilon = -\epsilon$  is the matter Lagrangian,  $\epsilon$  is the proper energy density, and  $\chi(\epsilon)$  represents the multiplicative gravity-matter coupling, which in the low energy limit tends to  $\chi(\epsilon \rightarrow 0) \sim \Lambda_0/\epsilon + 8\pi G_0$ , where  $\Lambda_0$  is the cosmological constant.

To derive the field equations with respect to  $g_{\mu\nu}$ , we apply the Fock method [91], where the density  $\epsilon$  is expressed in the form

$$\epsilon = \rho(1 + \Pi(\rho)), \quad \Pi(\rho) = \int \frac{dp(\rho)}{\rho} - \frac{p(\rho)}{\rho}, \quad (5)$$

where  $\Pi(\rho)$  is the internal energy per unit rest mass, and  $\rho$  is the rest mass density which satisfies the continuity equation  $\nabla_\mu(\rho u^\mu) = 0$ . One can write a relation between the variation of the proper energy density  $\epsilon$  and the rest mass energy density  $\rho$ , which is given by  $\delta\epsilon/\delta\rho = (p(\epsilon) + \epsilon)/\rho$ . Moreover, it has been shown [90] that the variation of the rest mass density with respect to the metric yields  $\delta\rho/\delta g^{\mu\nu} = \rho(g_{\mu\nu} + u_\mu u_\nu)/2$ .

By reading  $\delta\rho$  and substituting it into  $\delta\epsilon$ , we obtain an equation that describes the variation of the proper energy density with respect to the metric as a function of the pressure and the other geometric elements. It is written as

$$\delta\epsilon = \frac{p(\epsilon) + \epsilon}{2} (g_{\mu\nu} + u_\mu u_\nu) \delta g^{\mu\nu}, \quad (6)$$

for EOS  $p(\epsilon) = -\epsilon$ , the variation of the proper energy density vanishes  $\delta\epsilon = 0$ , which shows that the proper energy density remains constant. Consequently, the term  $\chi(\epsilon)\epsilon$  in the Lagrangian (4) is also a constant, effectively playing the role of the cosmological constant in the Einstein-Hilbert action. This EOS predicts a de Sitter or anti-de Sitter spacetime, depending on the sign of  $\chi(\epsilon)$ .

The metric variation of the matter part of the Lagrangian gives

$$\delta(2\sqrt{-g}\chi\epsilon) = \sqrt{-g} \left( 2 \frac{\partial(\chi\epsilon)}{\partial\epsilon} \delta\epsilon - \chi\epsilon g_{\mu\nu} \delta g^{\mu\nu} \right), \quad (7)$$

substituting the variation of the proper energy density Eq. (6) into Eq. (7) and considering the variation of the action (4) leads to the following field equations:

$$G_{\mu\nu} = \frac{\partial(\chi\epsilon)}{\partial\epsilon} T_{\mu\nu} + \epsilon^2 \frac{\partial\chi}{\partial\epsilon} g_{\mu\nu}. \quad (8)$$

This is an interesting result, it is well-known that the Einstein-Hilbert action when including a cosmological constant leads to a field equation with an additional matter-like term proportional to the metric field, expressed as  $G_{\mu\nu} \sim G_0 T_{\mu\nu} + \Lambda_0 g_{\mu\nu}$ . This is the most widely accepted field equation for gravity, but the cosmological constant is typically introduced into the Lagrangian by hand. In contrast, there is no explicit term for the cosmological constant in the action (4). There are the Ricci scalar and the matter terms in the action (4), both of which must be included according to the principles of general relativity [92].

By comparing Eq. (1) and Eq. (8), the following relationships can be derived

$$8\pi G(\epsilon) = \frac{\partial(\chi\epsilon)}{\partial\epsilon}, \quad \Lambda(\epsilon) = -\epsilon^2 \frac{\partial\chi}{\partial\epsilon}, \quad (9)$$

if the functional form of  $G(\epsilon)$  were known, the corresponding values of  $\chi(\epsilon)$  and  $\Lambda(\epsilon)$  could be determined as functions of the proper energy density. Following Refs. [14, 32], we adopt the approximate running of  $G$  derived from AS gravity in the context of quantum Einstein gravity in the appropriate limit

$$G(k) = \frac{G_0}{1 + G_0 k^2 / g_*}, \quad (10)$$

where  $k$  represents the infrared (IR) regulator scale, and  $g_* = 570\pi/833$  is the UV fixed point. Figure 1 shows the variation of the running gravitational coupling with respect to the momentum scale according to Eq. (10). The momentum scale has been shown to depend on the

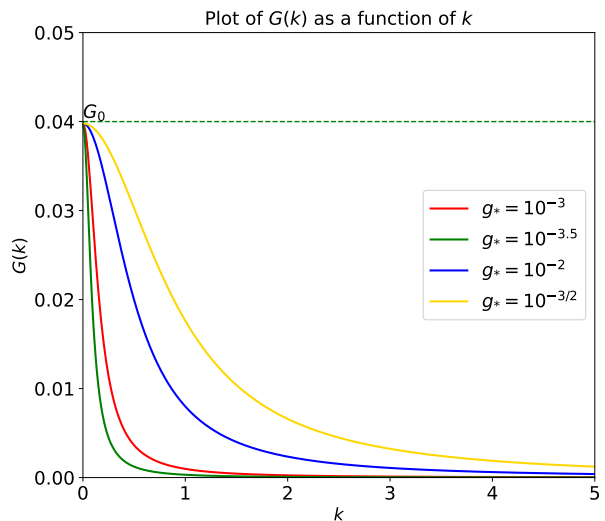


FIG. 1. The behaviour of  $G(k)$  as a function of the momentum scale  $k$  for different values of  $g_*$ , with  $8\pi G_0 = 1$ . At higher energy scales, the running gravitational coupling decreases, while at sufficiently low energy scales, it asymptotically approaches to  $1/8\pi$ .

distance as  $k(P) = \varpi/d(P)$ , where  $\varpi$  is a numerical constant, and  $d(P)$  represents the proper distance (measured with respect to the classical Schwarzschild metric) from the point  $P$  to the center of the BH along a curve  $\mathcal{C}$  (see Ref. [32]). The proper distance is defined as  $d(P) = \int_{\mathcal{C}} \sqrt{|ds^2|}$ . For a spherically symmetric spacetime, the proper distance depends only on the radial coordinate, i.e.,  $d(P) = d(R)$ . In the UV limit, this distance has been calculated as:  $d(R) = 2/(3\sqrt{2G_0 m_0})R^{3/2}$ , where  $m_0$  has the dimension of mass and ensures dimensional consistency [32]. Using this result, the IR regulator scale becomes  $k(R) = (3\beta/2)R^{-3/2}$ , where  $\beta = \varpi\sqrt{2G_0 m_0}$ . Substituting this into Eq. (10), the running gravitational coupling as a function of the radius is given by

$$G(R) = \frac{G_0}{1 + \varrho G_0 R^{-3}}, \quad (11)$$

where  $\varrho = 9\beta^2/(4g_*)$ . Figure 2 shows the variation of the running gravitational coupling as a function of radial distance according to Eq. (11).

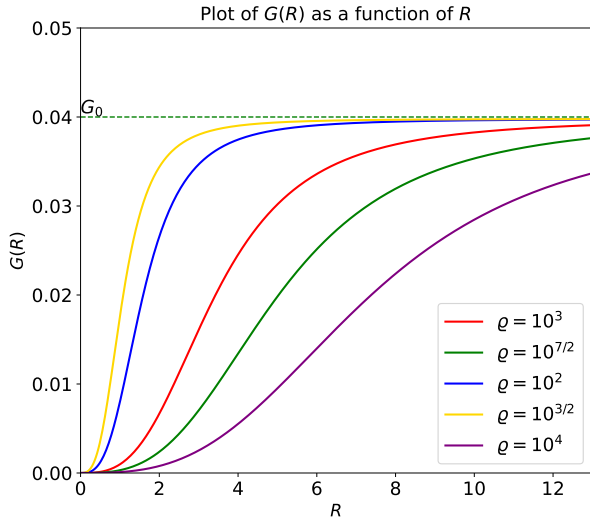


FIG. 2. The behaviour of  $G(R)$  as a function of the radial distance  $R$  for different values of  $\varrho$ , with  $8\pi G_0 = 1$ . The running gravitational coupling decreases at small distances, while it approaches to  $1/8\pi$  at sufficiently large distances.

Here, we focus on the study of the Oppenheimer-Snyder (OS) gravitational collapse in the context of a running gravitational coupling. Recently, the gravitational dust collapse in AS gravity has been studied in Ref. [64] with a running  $G(k)$  and  $\Lambda(k)$ . The authors show that, while satisfying all energy conditions, the running cosmological constant leads to repulsive effects, thus avoiding the singularity. In this paper, we first extend the analysis in Ref. [64] to the case where the stellar perfect fluid matter has the pressure. Second, we investigate various BH solutions along with FLRW spacetime for different equations of state. To achieve this, we will study the gravitational collapse within the framework of AS gravity. We take the interior of the star as a homogeneous and isotropic spacetime described by the FLRW metric

$$ds_-^2 = -d\tau^2 + \frac{a^2(\tau)}{1 - kr^2} dr^2 + a^2(\tau)r^2 d\Omega^2, \quad (12)$$

where  $\tau$  and  $r$  denote the comoving time and radial coordinates, respectively. The spacetime outside the star is described by the static spherically symmetric metric in  $(t, R, \theta, \phi)$  coordinates

$$ds_+^2 = -f(R)dt^2 + f^{-1}(R)dR^2 + R^2 d\Omega^2, \quad (13)$$

where  $f(R) = 1 - 2m(R)/R$ . The two metrics inside and outside the star, are smoothly joined at the hypersurface  $\Sigma$ , which serves as the boundary of the star. Thus, from the outside, the collapsing boundary of the star is

described by the parametric equations  $R = R_b(\tau)$  and  $t = T(\tau)$ , with the following induced metric

$$ds_\Sigma^2 = -(f(R_b)\dot{T}^2 - f^{-1}(R_b)\dot{R}_b^2)d\tau^2 + R_b^2 d\Omega^2, \quad (14)$$

where an overdot indicates differentiation with respect to  $\tau$ . The hypersurface  $\Sigma$  coincides with the surface of the collapsing star, which is located at  $r_b = \text{constant}$  in the comoving coordinate system. Thus, from the inside, the induced metric on the comoving boundary  $r_b$  is expressed as follows

$$ds_\Sigma^2 = -d\tau^2 + a^2(\tau)r_b^2 d\Omega^2. \quad (15)$$

To ensure a smooth transition between the inner and outer geometries, we require that the metric and its first derivatives remain continuous over the surface of the star. The last condition is equivalent to requiring that the extrinsic curvatures  $K_{\alpha\beta}$  of the inner and outer geometries match at the surface. These continuity conditions are known as the *Israel junction conditions* [93]. The second fundamental forms of the inner and outer metrics are given by

$$K_{\tau\tau}^- = 0, \quad K_{\theta\theta}^- = r_b a(\tau) \sqrt{1 - kr_b^2} \quad (16)$$

$$K_{\tau\tau}^+ = -\frac{\dot{\Delta}(R_b)}{\dot{R}_b}, \quad K_{\theta\theta}^+ = R_b \Delta(R_b), \quad (17)$$

where  $\Delta(R_b) = \sqrt{1 - 2m(R_b)/R_b + \dot{R}_b^2}$ . To achieve a smooth joining of the two geometries, the components of the metric and the second fundamental form must remain continuous across  $\Sigma$ . This leads to

$$R_b = a(\tau)r_b, \quad (18)$$

$$\dot{T} = \frac{\Delta(R_b)}{f(R_b)}, \quad (19)$$

$$\Delta(R_b) = \sqrt{1 - kr_b^2} = \text{constant}, \quad (20)$$

$$H^2(\tau) + \frac{k}{a^2(\tau)} = \frac{2m(R_b)}{R_b^3}, \quad (21)$$

these dynamical equations will be used to investigate various properties and definitions associated with the BH spacetime in Eq. (13). For example, by applying the Friedmann equations inside a collapsing star, we can calculate its Misner-Sharp (MS) mass as a function of the radius  $R_b$  using Eq. (21). We will develop this analysis further in the following sections, but first it is important to establish some basic concepts.

By differentiating Eq. (8) and Eq. (9) with respect to  $\epsilon$ , and then substituting the results into the Bianchi identity  $\nabla_\mu T_{\text{eff}}^{\mu\nu} = 0$  the energy-momentum conservation law for  $T^{\mu\nu}$  is easily derived as follows

$$\nabla_\mu T^{\mu\nu} = -\frac{\partial \epsilon}{\partial x^\mu} \frac{G'(\epsilon)}{G(\epsilon)} (\epsilon + p)(u^\mu u^\nu + g^{\mu\nu}), \quad (22)$$

noting that the comoving energy density depends only on time,  $\epsilon = \epsilon(\tau)$ . Using the four-velocity in the comoving

frame,  $u^\mu = \delta_0^\mu$ , and the FLRW metric (12), the energy-momentum conservation Eq. (22) simplifies to  $\nabla_\mu T^{\mu\nu} = 0$ , which reduces to  $d\epsilon + 3(\epsilon + p(\epsilon))d\ln a = 0^1$ , with the solution

$$\epsilon = \epsilon_0 a^{-3(1+w)}, \quad (23)$$

for a linear EOS  $p(\epsilon) = w\epsilon$ .

Inside the star, the gravitational field equations (1), which include the effective cosmological fluid, take the form of the standard Friedmann equations

$$H^2 + \frac{k}{a^2} = \frac{8\pi}{3}\rho_e, \quad (24a)$$

$$\dot{H} + H^2 = -\frac{4\pi}{3}(\rho_e + 3p_e), \quad (24b)$$

and the effective energy conservation law is satisfied:  $d\rho_e + 3(\rho_e + p_e)d\ln a = 0$ . Comparing Eq. (21) with Eq. (24a) at the surface of the star, gives the effective energy density as a function of the star's radius

$$\rho_e = \frac{3}{4\pi} \frac{m(R_b)}{R_b^3}, \quad p_e = -\frac{m'(R_b)}{4\pi R_b^2}, \quad (25)$$

using the energy conservation equation for the effective pressure. For the exterior of the star, substituting Eq. (13) into Einstein's equations (1) gives the expressions for the density and the components of the anisotropic pressures as follows

$$\rho_{\text{out}} = -p_{\text{out}}^{(R)} = \frac{m'(R)}{4\pi R^2}, \quad p_{\text{out}}^{(\theta)} = p_{\text{out}}^{(\phi)} = -\frac{m''(R)}{8\pi R}. \quad (26)$$

Furthermore, by using Eq. (25) and Eq. (26), one can easily calculate the pure radial pressure at the star's surface as follows

$$p_{\text{star}}^{(r)} = p_e|_{R_b} - p_{\text{out}}^{(r)}|_{R_b} = 0, \quad p_{\text{star}}^{(\theta)}|_{R_b} = p_{\text{star}}^{(\phi)}|_{R_b} \neq 0, \quad (27)$$

this indicates that the boundary surface of the star is characterized by zero pure radial pressure, allowing each particle to follow the radial geodesic in accordance with the effective energy-momentum continuity equation.

We can determine the running gravitational coupling for a collapsing star with non-zero pressure by focusing on the star's surface,  $R = R_b = a(\tau)r_b$ . Substituting this expression into the distance-dependent gravitational coupling given by Eq. (11),  $G(R)$ , we can express the gravitational coupling as a function of the scale factor,  $G(a)$ . Furthermore, by substituting Eq. (23) into the gravitational coupling  $G(a)$ , which depends on the scale

factor, gives the gravitational coupling as a function of the proper energy density, as follows

$$G_w(\epsilon) = \frac{G_0}{1 + \alpha G_0 \epsilon^{\frac{1}{1+w}}}, \quad (28)$$

where  $\alpha = \varrho \epsilon_0^{-1/(1+w)} r_b^{-3}$  and  $r_b$  is the comoving radius. We derived the energy density-dependent gravitational coupling, Eq. (28), using the Israel junction conditions. A similar equation has been conjectured in the literature; see Ref. [95]<sup>2</sup>. The running gravitational coupling is now expressed as a function of the proper energy density. This relationship varies according to the EOS, with each equation yielding a different functional form for the running gravitational coupling. These variations are essential for understanding the behavior of gravitational interactions under different physical conditions, especially in cosmological and high-energy regimes.

Figure 3 illustrates the variation of the running gravitational coupling Eq. (28) as a function of the energy density  $\epsilon$  and  $w$ .

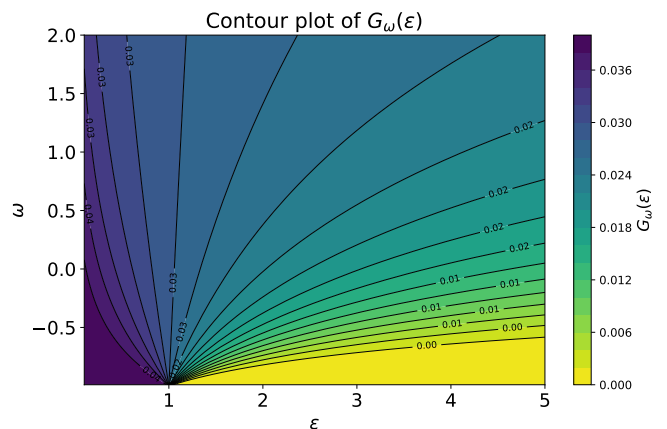


FIG. 3. Contours of  $G_w(\epsilon)$  with respect to the parameters  $\epsilon$  and  $w$ . Lighter regions represent lower values of  $G_w(\epsilon)$ , while darker regions represent higher values.  $G_w(\epsilon)$  generally decreases as  $\epsilon$  increases. The rate of decrease is significantly affected by  $w$ . Contour lines highlight regions of constant  $G_w(\epsilon)$ , providing a detailed view of the function's behavior in parameter space. The parameters are set as  $8\pi G_0 = 1$  and  $\alpha = 10$ .

Substituting Eq. (28) into Eq. (8), we obtain expressions for  $\chi(\epsilon)$  and  $\Lambda(\epsilon)$  as follows

$$\chi_w(\epsilon) = \frac{\Lambda_0}{\epsilon} + 8\pi G_0 {}_2F_1(1, 1+w; 2+w; -\alpha G_0 \epsilon^{\frac{1}{1+w}}), \quad (29)$$

<sup>1</sup> Some suggest that the cosmological constant can be neglected  $\Lambda(\epsilon) \simeq 0$  when studying local objects or systems, such as BHs [19, 94]. However, this has a significant consequence: the continuity equation becomes  $\dot{\epsilon} + 3H(\epsilon + p) = -\epsilon \dot{G}(\epsilon)/G(\epsilon)$ .

<sup>2</sup> The running gravitational coupling is expressed as  $G(\epsilon) = G_N [1 + \tilde{\omega}(G_N^2 \epsilon)^\alpha]^{-1}$ , where  $G_N$  denotes Newton's gravitational constant, and  $\alpha$  is a free parameter.

$$\Lambda_w(\epsilon) = \Lambda_0 + 8\pi G_0 \epsilon {}_2F_1(1, 1+w; 2+w; -\alpha G_0 \epsilon^{\frac{1}{1+w}}) - \frac{8\pi G_0 \epsilon}{1 + \alpha G_0 \epsilon^{\frac{1}{1+w}}}, \quad (30)$$

where  $w+2 \notin -\mathbb{N}$ , and  $\Lambda_0$  is the integration constant that plays the role of the cosmological constant (zero point energy  $\Lambda_w(\epsilon=0) = \Lambda_0$ ).

Furthermore, it is easy to analyze the expressions in Eq. (29) and Eq. (30) at both low and high energy densities. For a small energy density  $\epsilon \ll (\alpha G_0)^{-(1+w)}$ , they are simplified to

$$\chi(\epsilon) \simeq \frac{\Lambda_0}{\epsilon} + 8\pi G_0, \quad \Lambda(\epsilon) \simeq \Lambda_0, \quad (31)$$

substituting these into Eq. (8) yields

$$G_{\mu\nu} \simeq 8\pi G_0 T_{\mu\nu} - \Lambda_0 g_{\mu\nu}, \quad (32)$$

which is Einstein's field equations for a perfect fluid in the presence of a cosmological constant.

We now have the explicit functions for the matter-gravity coupling,  $\chi_w(\epsilon)$ , and the running cosmological constant,  $\Lambda_w(\epsilon)$ . These functions serve as the fundamental components necessary to analyze a system via the action described in Eq. (4).

Figure 4 illustrates the gravity-matter coupling,  $\chi_w(\epsilon)$ , as a function of the energy density  $\epsilon$  and the parameter  $w$ . Similarly, Fig. 5 presents the behavior of the running cosmological constant,  $\Lambda_w(\epsilon)$ , plotted against the energy density  $\epsilon$  and the parameter  $w$ .

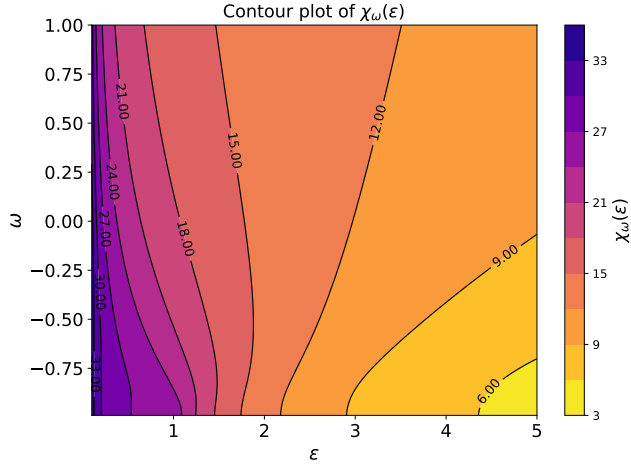


FIG. 4. Contours of  $\chi_w(\epsilon)$  as a function of  $\epsilon$  and  $w$ . The color gradient indicates the value of  $\chi_w$ , with darker and lighter shades representing larger and smaller values, respectively. Contour lines mark points of equal value to show patterns and transitions in  $\chi_w(\epsilon)$ . The parameters are set as  $G_0 = \alpha = \Lambda_0 = 1$

In the following, assuming some specific values of  $w$ , we will further study Eq. (29) and Eq. (30).

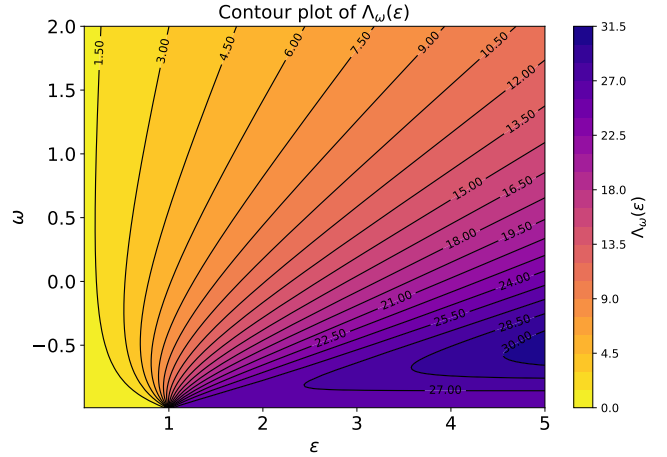


FIG. 5. Contours of  $\Lambda_w(\epsilon)$  as a function of energy density  $\epsilon$  and parameter  $w$ . The contour lines represent regions with constant values of  $\Lambda_w(\epsilon)$ . The color gradient indicates the magnitude of  $\Lambda_w(\epsilon)$ , with darker regions corresponding to higher values. The parameters are set as  $\Lambda_0 = G_0 = \alpha = 1$ .

### 1. $w = 0$

For dust matter with  $w = 0$ , Eq. (29) and Eq. (30) reduce to

$$\chi(\epsilon) = \frac{\Lambda_0}{\epsilon} + \frac{8\pi \ln(1 + \alpha G_0 \epsilon)}{\epsilon}, \quad (33)$$

$$\Lambda(\epsilon) = \Lambda_0 + \frac{8\pi}{\alpha} \ln(1 + \alpha G_0 \epsilon) - \frac{8\pi G_0 \epsilon}{1 + \alpha G_0 \epsilon}, \quad (34)$$

these equations were derived using Eq. (A10). By substituting Eq. (33) and Eq. (34) into Eq. (1), we derive the effective pressure  $p_e$  and the effective energy density  $\rho_e$  given by

$$\rho_e = \frac{\Lambda_0}{8\pi} + \frac{\ln(1 + \alpha G_0 \epsilon)}{\alpha}, \quad (35)$$

$$p_e = -\frac{\Lambda_0}{8\pi} - \frac{\ln(1 + \alpha G_0 \epsilon)}{\alpha} + \frac{G_0 \epsilon}{1 + \alpha G_0 \epsilon}, \quad (36)$$

combining these equations leads to the following effective EOS

$$p_e = -\rho_e - \frac{e^{\alpha(\Lambda_0/8\pi - \rho_e)} - 1}{\alpha}, \quad (37)$$

expanding this effective EOS around  $\rho_e = \Lambda_0/8\pi$  yields the following form

$$p_e \simeq -\frac{\Lambda_0}{8\pi} - \frac{\alpha \Lambda_0^2}{128\pi^2} + \frac{\alpha \Lambda_0}{8\pi} \rho_e - \frac{\alpha}{2} \rho_e^2, \quad (38)$$

on the right-hand side, there is a second-degree (quadratic) negative pressure, which corresponds to a polytropic equation of state with index  $n = 1$ . Such a

negative equation of state has been identified in the gravitational collapse leading to the formation of a Hayward regular BH<sup>3</sup>.

At high effective energy densities, where  $\rho_e \gg \Lambda_0/8\pi$ , the effective EOS (37) approaches  $p_e \simeq -\rho_e$ . Furthermore, when  $\rho_e = \Lambda_0/8\pi$ , it reduces exactly to  $p_e = -\rho_e$ . These results are indeed intriguing; at high energy densities and for a certain value of the effective energy density we obtain a de Sitter (or anti-de Sitter) spacetime. Additionally, when the effective energy density is zero, the effective pressure becomes constant and is expressed as  $p_e = (1 - e^{\alpha\Lambda_0/8\pi})/\alpha$ , where the effective pressure is negative for a positive cosmological constant  $\Lambda_0 > 0$  and positive for a negative cosmological constant  $\Lambda_0 < 0$ . In the limit  $\alpha \rightarrow 0$ , this pressure tends to

$$p_e = \lim_{\alpha \rightarrow 0} \frac{1 - e^{\alpha\Lambda_0/8\pi}}{\alpha} = -\frac{\Lambda_0}{8\pi}. \quad (39)$$

The effective pressure described by Eq. (37) exhibits both positive and negative signs for different values of the effective energy density, which is crucial for understanding the underlying physics. The conditions that lead to a sign change of the effective pressure are as follows

- $p_e < 0$  if  $e^{\alpha(\frac{\Lambda_0}{8\pi} - \rho_e)} > 1 - \alpha\rho_e$ ,
- $p_e > 0$  if  $\{e^{\alpha(\frac{\Lambda_0}{8\pi} - \rho_e)} < 1 - \alpha\rho_e, \rho_e < \frac{1}{\alpha}\}$ .

The critical effective energy density  $\rho_c = 1/\alpha$  is of considerable importance. When the effective energy density is below this critical threshold, the effective pressure can be positive. However, once  $\rho_e$  exceeds  $\rho_c$ , the effective pressure becomes definitively negative. This negative pressure can play a crucial role in facilitating the creation of non-singular spacetime at high energy densities. Fig. 6 illustrates the general behavior of the effective pressure in Eq. (37) as a function of the effective energy density.

## 2. $w = -1$

Among the various possible linear EOS, the case  $w = -1$  exhibits unique properties, which will be demonstrated in this paper through various calculations. In the limit  $w \rightarrow -1$ , we find

$$\lim_{w \rightarrow -1^+} -\frac{8\pi G_0 \epsilon}{1 + \alpha G_0 \epsilon^{\frac{1}{1+w}}} = \begin{cases} 0 & \text{if } \epsilon > 1, \\ -8\pi G_0 \epsilon & \text{if } 0 < \epsilon < 1 \end{cases} \quad (40)$$

and

$${}_2F_1(1, 1+w; 2+w; -\alpha G_0 \epsilon^{\frac{1}{1+w}}) \Big|_{w \rightarrow -1} = 1, \quad (41)$$

<sup>3</sup> In the case of a Hayward BH, the stellar matter is described by a polytropic fluid with equation of state  $p \propto \rho^{1+1/n}$ , where the polytropic index  $n$  is equal to unity. This leads to the specific form  $p = -\frac{8\pi}{3} l^2 \rho^2$  (see Ref. [18]).

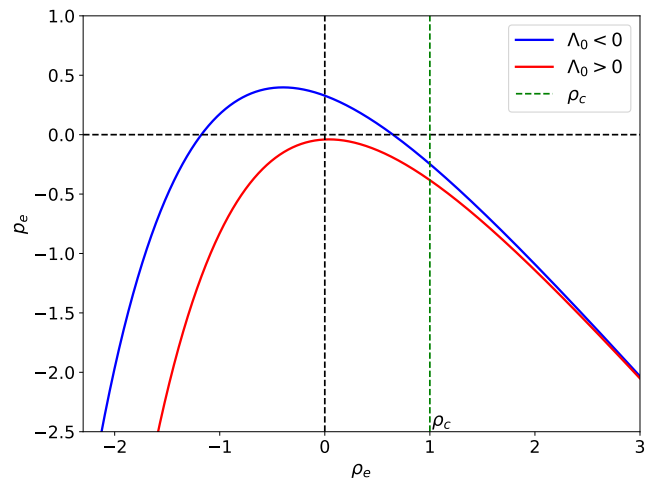


FIG. 6. Pressure  $p_e$  as a function of the energy density  $\rho_e$  for two cases:  $\Lambda_0 > 0$  (red curve) and  $\Lambda_0 < 0$  (blue curve). The vertical dashed green line marks the critical energy density  $\rho_c$ . This plot illustrates the dependence of the pressure on the energy density under different cosmological constant regimes. The parameters are set as  $\Lambda_0 = 1$  (positive value),  $\Lambda_0 = -10$  (negative value), and  $\alpha = 1$ .

substituting these equations into Eq. (29) and Eq. (30) leads to two different scenarios

- $\epsilon > 1$

$$\chi(\epsilon) = \frac{\Lambda_0}{\epsilon} + 8\pi G_0, \quad \Lambda(\epsilon) \simeq \Lambda_0 + 8\pi G_0 \epsilon, \quad (42)$$

inserting these equations into Einstein's field equations (8) yields

$$G_{\mu\nu} \simeq -(\Lambda_0 + 16\pi G_0 \epsilon_0) g_{\mu\nu}, \quad (43)$$

this is the Einstein vacuum field equation with a cosmological constant.

- $0 < \epsilon < 1$

$$\chi(\epsilon) = \frac{\Lambda_0}{\epsilon} + 8\pi G_0, \quad \Lambda(\epsilon) \simeq \Lambda_0, \quad (44)$$

similarly, substituting these equations into Einstein's field equations (8) yields

$$G_{\mu\nu} \simeq -(\Lambda_0 + 8\pi G_0 \epsilon_0) g_{\mu\nu}, \quad (45)$$

this equation illustrates the Einstein field equations when a cosmological constant and an integration constant are included.

Indeed, when  $w = -1$ , the gravitational field equations given by Eq. (1) correspond to a de Sitter (or anti-de Sitter) spacetime characterized by distinct constant values in the high and low energy density limits.

3.  $w = 1$ 

An important and well-known EOS is characterized by  $w = 1$  [96]. For this EOS, Eq. (29) and Eq. (30) are simplified as

$$\chi_1(\epsilon) = \frac{\Lambda_0}{\epsilon} + \frac{16\pi}{\alpha\sqrt{\epsilon}} - \frac{16\pi \ln(1 + \alpha G_0 \sqrt{\epsilon})}{\alpha^2 G_0 \epsilon}, \quad (46)$$

$$\Lambda_1(\epsilon) = \Lambda_0 + \frac{8\pi\sqrt{\epsilon}}{\alpha} \frac{2 + \alpha G_0 \sqrt{\epsilon}}{1 + \alpha G_0 \sqrt{\epsilon}} - \frac{16\pi \ln(1 + \alpha G_0 \sqrt{\epsilon})}{\alpha^2 G_0}, \quad (47)$$

to derive the above equations, we used Eq. (A16). Inserting Eq. (46) and Eq. (47) into Eq. (1) gives the following equations for the effective pressure and effective energy density

$$\rho_e = \frac{G_0 \epsilon}{1 + \alpha G_0 \sqrt{\epsilon}} + \frac{\Lambda_1(\epsilon)}{8\pi}, \quad (48)$$

$$p_e = \frac{G_0 \epsilon}{1 + \alpha G_0 \sqrt{\epsilon}} - \frac{\Lambda_1(\epsilon)}{8\pi}. \quad (49)$$

In general, deriving an analytical expression for the effective EOS by combining Eq. (48) and Eq. (49) is not feasible. However, for small energy densities,  $\epsilon \ll (\alpha G_0)^{-2}$ , the effective EOS can be approximated as follows

$$p_e \simeq \rho_e - \frac{\Lambda_0}{4\pi} - 2\alpha\sqrt{G_0} \left( \rho_e - \frac{\Lambda_0}{8\pi} \right)^{3/2}, \quad (50)$$

where the third term on the right-hand side has the familiar form of a polytropic EOS<sup>4</sup>. For  $\rho_e = \Lambda_0/8\pi$ , Eq. (50) reduces to  $p_e = -\rho_e$ .

For high energy densities, where  $\epsilon \gg (\alpha G_0)^{-2}$ , the EOS can be derived from Eq. (48) and Eq. (49) as

$$(p_e + \rho_e) e^{-\alpha^2 G_0 (3p_e + \rho_e)/4} \simeq \frac{2}{\alpha^2 G_0} e^{\alpha^2 G_0 \Lambda_0 / 16\pi}. \quad (51)$$

Figure 7 shows the general relationship between the effective pressure, given by Eq. (51) and the effective energy density. It demonstrates that the pressure in the effective equations of state (51) is positive in the low-energy density limit and becomes negative at high energy densities. The negative pressure at high energy densities can slow down the collapse of the star or, in certain cases, prevent the formation of a singularity in the final stage of gravitational collapse [18].

<sup>4</sup> The polytropic EOS,  $p = K\rho^\gamma$ , where  $p$  is the pressure,  $\rho$  is the density, and  $\gamma = 1 + 1/n$ , (where  $n$  is the polytropic index), and  $K$  is a proportionality constant, provides a simplified model to describe the thermodynamic behavior of self-gravitating fluids. By defining  $\bar{\rho}_e = \rho_e - \Lambda_0/8\pi$ , the effective EOS (50), becomes  $p_e \simeq -\Lambda_0/8\pi + \bar{\rho}_e + K\bar{\rho}_e^{3/2}$ , where the third term corresponds to a polytropic EOS with a polytropic index  $n = 2$  and  $K = -2\alpha\sqrt{G_0}$ .

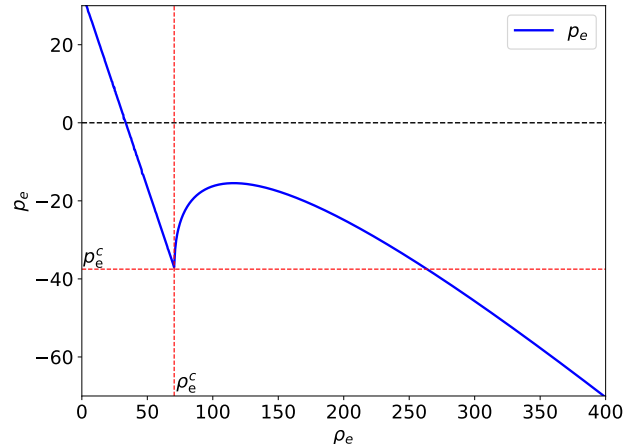


FIG. 7. Effective pressure  $p_e$  as a function of the effective energy density  $\rho_e$  according to Eq. (51). The parameters are set as  $8\pi G_0 = 1$ , and  $\alpha = \Lambda_0 = 1$ .

Figure 7 illustrates a discontinuity in the pressure equation as a function of the effective energy density, as described by Eq. (51). To investigate this behavior in greater detail, we differentiate both sides of Eq. (51) with respect to  $\rho_e$ , yielding

$$\frac{dp_e}{d\rho_e} = -\frac{4 - \alpha^2 G_0 (p_e + \rho_e)}{4 - 3\alpha^2 G_0 (p_e + \rho_e)}, \quad (52)$$

a discontinuity occurs where the denominator vanishes, it leads to

$$p_e^c = -\rho_e^c + \frac{4}{3\alpha^2 G_0}, \quad (53)$$

here  $p_e^c$  denotes the critical effective pressure, and  $\rho_e^c$  represents the critical effective energy density.

4.  $w = \frac{1}{2}$ 

Another important case is  $w = 1/2$  where Eq. (29) and Eq. (30) are simplified as

$$\chi_{1/2}(\epsilon) = \frac{\Lambda_0}{\epsilon} + \frac{24\pi}{\alpha\epsilon} \left( \epsilon^{1/3} - \frac{\arctan(\sqrt{\alpha G_0} \epsilon^{1/3})}{\sqrt{\alpha G_0}} \right), \quad (54)$$

$$\Lambda_{1/2}(\epsilon) = \Lambda_0 + \frac{24\pi}{\alpha} \left( \epsilon^{1/3} - \frac{\arctan(\sqrt{\alpha G_0} \epsilon^{1/3})}{\sqrt{\alpha G_0}} \right) - \frac{8\pi G_0 \epsilon}{1 + \alpha G_0 \epsilon^{\frac{2}{3}}}, \quad (55)$$

to derive these equations, we applied Eq. (A20). Substituting Eq. (54) and Eq. (55) into Eq. (1) gives the following expressions for the effective pressure and effective

energy density

$$\rho_e = \frac{G_0\epsilon}{1 + \alpha G_0\epsilon^{2/3}} + \frac{\Lambda_{1/2}(\epsilon)}{8\pi}, \quad (56)$$

$$p_e = \frac{G_0\epsilon}{2(1 + \alpha G_0\epsilon^{2/3})} - \frac{\Lambda_{1/2}(\epsilon)}{8\pi}, \quad (57)$$

it is not possible to combine these equations to obtain an analytic effective EOS, but they can be analyzed in the low- and high-energy density limits. Therefore, in the small energy density limit  $\epsilon \ll (\alpha G_0)^{-3/2}$ , we approximate  $\arctan(x)$  as  $\arctan(x) \simeq x - x^3/3$ . By combining Eq. (56) and Eq. (57), we derive the following equation of state

$$p_e \simeq \frac{\rho_e}{2} - \frac{3\Lambda_0}{16\pi} - \frac{3}{2}\alpha G_0^{1/3} \left( \rho_e - \frac{\Lambda_0}{8\pi} \right)^{5/3}, \quad (58)$$

the third term on the right-hand side takes the familiar form of a polytropic EOS<sup>5</sup>, which has been observed in the gravitational collapse of an old star into Bardeen spacetime (see Ref. [18])<sup>6</sup>.

At high energy density limit,  $\epsilon \gg (\alpha G_0)^{-3/2}$ , Eq. (56) and Eq. (57) can be combined to give the following effective EOS

$$p_e \simeq -\frac{1}{2}\rho_e + \frac{1}{4} \left( \frac{3\pi}{\alpha\sqrt{\alpha G_0}} - \frac{\Lambda_0}{4\pi} \right), \quad (59)$$

at high effective energy density, this equation of state approaches  $p_e \simeq -\rho_e/2$ , where a similar equation of state at high energy densities has been found in the gravitational collapse of a massive object described by the 4D Einstein-Gauss-Bonnet (4D-EGB) theory of gravity<sup>7</sup>.

5.  $w = -\frac{1}{2}$

Another notable case is  $w = -1/2$ , where Eq. (29) and Eq. (30) simplify to

$$\chi_{(-1/2)}(\epsilon) = \frac{\Lambda_0}{\epsilon} + 8\pi\sqrt{\frac{G_0}{\alpha}} \frac{\arctan(\sqrt{\alpha G_0}\epsilon)}{\epsilon}, \quad (61)$$

<sup>5</sup> Defining  $\bar{\rho}_e = \rho_e - \Lambda_0/8\pi$ , the effective equation of state in Eq. (58) takes the form  $p_e \simeq -\Lambda_0/8\pi + \bar{\rho}_e/2 + K\bar{\rho}_e^{5/3}$ , where the third term represents a polytropic equation of state with a polytropic index  $n = 3/2$  and  $K = -3\alpha G_0^{1/3}/2$ .

<sup>6</sup> For the Bardeen BH, the stellar matter is modeled as a polytropic fluid governed by the equation of state  $p = -(4\pi/3m)^{2/3}g^2\rho^{5/3}$ .

<sup>7</sup> The gravitational collapse in 4D-EGB [20], predicts the stellar equation of state as

$$\bar{\rho}^{\text{eff}} = -\frac{128\pi^2\tilde{\alpha}(\bar{\rho}^{\text{eff}})^2}{3} \left( 1 + \frac{256\pi^2\tilde{\alpha}}{3}\bar{\rho}^{\text{eff}} \right)^{-1}, \quad (60)$$

for sufficiently large density, Eq. (60) reduces to the linear equation of state  $\bar{\rho}^{\text{eff}} = -\bar{\rho}^{\text{eff}}/2$ .

$$\Lambda_{(-1/2)}(\epsilon) = \Lambda_0 + 8\pi\sqrt{\frac{G_0}{\alpha}} \arctan(\sqrt{\alpha G_0}\epsilon) - \frac{8\pi G_0\epsilon}{1 + \alpha G_0\epsilon^2}, \quad (62)$$

to obtain these equations, we employed Eq. (A11). Substituting Eq. (61) and Eq. (62) into Eq. (1), we obtain the following expressions for the effective pressure and energy density

$$\rho_e = \frac{G_0\epsilon}{1 + \alpha G_0\epsilon^2} + \frac{\Lambda_{(-1/2)}(\epsilon)}{8\pi}, \quad (63)$$

$$p_e = -\frac{G_0\epsilon}{2(1 + \alpha G_0\epsilon^2)} - \frac{\Lambda_{(-1/2)}(\epsilon)}{8\pi}, \quad (64)$$

at low energy density limit,  $\epsilon \ll (\alpha G_0)^{-2}$ , the effective EOS can be expressed analytically by combining Eq. (63) and Eq. (64), yielding

$$p_e \simeq -\frac{1}{2}\rho_e - \frac{\Lambda_0}{16\pi} - \frac{\alpha}{2G_0} \left( \rho_e - \frac{\Lambda_0}{8\pi} \right)^3, \quad (65)$$

the third term on the right-hand side corresponds to a polytropic equation of state<sup>8</sup>.

For the high-energy density limit,  $\epsilon \gg (\alpha G_0)^{-2}$ , Eq. (63) and Eq. (64) can be combined to yield the effective EOS,

$$p_e \simeq -\frac{3}{2}\rho_e + \frac{\Lambda_0}{16\pi} + \frac{\pi}{4}\sqrt{\frac{G_0}{\alpha}}, \quad (66)$$

## 6. $|w| \gg 1$

In the limit  $|w| \gg 1$ , Eq. (29) and Eq. (30) reduce to

$$\chi_w(\epsilon) = \frac{\Lambda_0}{\epsilon} + \frac{8\pi G_0}{1 + \alpha G_0\epsilon^{\frac{1}{w}}}, \quad \Lambda_w \simeq \Lambda_0, \quad (67)$$

to obtain the above equation, we used Eq. (A9). The first important result of these equations is that the running cosmological constant simply becomes a constant. By substituting them into Eq. (1), we obtain

$$\rho_e = \frac{\Lambda_0}{8\pi}, \quad (68)$$

$$p_e = \frac{G_0 w \epsilon}{1 + \alpha G_0 \epsilon^{\frac{1}{w}}} - \frac{\Lambda_0}{8\pi}, \quad (69)$$

the effective pressure Eq. (69) in the limit  $w \gg 1$  is given by

$$p_e \simeq \frac{G_0 w \epsilon}{1 + \alpha G_0} \left( 1 - \frac{\alpha G_0 \ln(\epsilon)}{(1 + \alpha G_0)w} \right) + O\left(\frac{1}{w^2}\right), \quad (70)$$

<sup>8</sup> By introducing  $\bar{\rho}_e = \rho_e - \Lambda_0/8\pi$ , the effective equation of state in Eq. (65) can be expressed as  $p_e \simeq -\Lambda_0/8\pi - \bar{\rho}_e/2 + K\bar{\rho}_e^3$ . Here, the third term corresponds to a polytropic equation of state with a polytropic index  $n = 1/2$  and  $K = -\alpha/(2G_0)$ .

as  $w$  approaches infinity, this pressure converges to  $p_e \simeq G_\infty w \epsilon$ , where

$$G_\infty = \frac{G_0}{1 + \alpha G_0}, \quad (71)$$

this can also be seen from Eq. (28). This shows that for a finite energy density, when the pressure diverges ( $w \rightarrow \pm\infty$ ), the running gravitational coupling approaches a constant, finite value  $G_\infty$ . However,  $G_\infty$  is smaller than the Newtonian gravitational constant  $G_0$ . The Newtonian gravitational constant is measured in the weak gravity regime, while Eq. (71) predicts a reduced value in the high-pressure limit (similar to conditions at the center of gravitationally collapsing objects or in the early universe).

### III. FRIEDMANN EQUATIONS

The study of FLRW spacetime dynamics is of great importance for any gravitational theory. It can describe the dynamics of our universe according to the cosmological principle and can be a reliable model for the interior of gravitationally collapsed objects. Therefore, in this section, we want to investigate the FLRW solutions of the gravitational field equations (8). Substituting the FLRW metric Eq. (12) into the field equation (8) together with the running coupling constant and the cosmological constant Eq. (28) and Eq. (30), gives us the Friedmann equations

$$H^2 + \frac{k}{a^2} = \frac{8\pi G_0 \epsilon}{3} {}_2F_1\left(1, 1+w; 2+w; -\alpha G_0 \epsilon^{\frac{1}{1+w}}\right), \quad (72)$$

where we assumed  $\Lambda_0 = 0$ . This equation reduces to the standard Friedmann equation  $H^2 + k/a^2 = 8\pi G_0 \epsilon/3$  in the limit  $\epsilon \ll (\alpha G_0)^{-(1+w)}$ . In the following analysis, we examine the Friedmann equation for various values of the EOS parameter.

- For a dust fluid,  $w = 0$ , the Friedmann equation (72) can be written according to Eq. (A10) as follows

$$H^2 + \frac{k}{a^2} = \frac{8\pi}{3\alpha} \ln(1 + \alpha G_0 \epsilon), \quad (73)$$

where tends to  $H^2 + k/a^2 \simeq (8\pi G_0 \epsilon/3)(1 - \epsilon/\epsilon_{cr})$  using the definition of  $\epsilon_{cr} = 2/(\alpha G_0)$  for sufficiently small energy density. The above equation is similar to the modified Friedmann equation in loop quantum cosmology [47], or the FLRW solution of the 4D Einstein–Gauss–Bonnet (EGB) theory of gravity<sup>9</sup>.

<sup>9</sup> The 4D EGB gravity theory proposed in Ref. [97] makes some significant predictions in both BH physics and cosmology [98]. Its Friedmann equations at small energy density becomes  $H^2 + \frac{k}{a^2} \simeq \frac{8\pi G_0 \epsilon}{3} \left(1 - \frac{64\pi \alpha G_0 \epsilon}{3}\right)$ .

- For the EOS parameter with  $w = -1/2$ , using Eq. (A11), the Friedmann equation (72) becomes

$$H^2 + \frac{k}{a^2} = \frac{8\pi}{3} \sqrt{\frac{G_0}{\alpha}} \arctan\left(\sqrt{G_0 \alpha} \epsilon\right), \quad (74)$$

at high energy density, Eq. (74) becomes  $H^2 + k/a^2 = \Lambda/3$ , where  $\Lambda = 8\pi \sqrt{G_0/\alpha}$ . This is the Friedmann equation in the presence of the cosmological constant. In the low energy density limit  $\epsilon \ll 1/\sqrt{G_0 \alpha}$ , Eq. (74) tends to  $H^2 + k/a^2 \simeq (8\pi G_0 \epsilon/3)(1 - \epsilon^2/\epsilon_{cr})$ , where  $\epsilon_{cr} = 3/(\alpha G_0)$ .

- For the EOS parameter with  $w = 1/2$ , the Friedmann equation (72) takes the form

$$H^2 + \frac{k}{a^2} = \frac{8\pi \epsilon^{\frac{1}{3}}}{\alpha} \left(1 - \frac{\arctan\left(\sqrt{\alpha G_0} \epsilon^{\frac{1}{3}}\right)}{\sqrt{\alpha G_0} \epsilon^{\frac{1}{3}}}\right), \quad (75)$$

at high energy density, Eq. (75) becomes  $H^2 + k/a^2 \simeq (8\pi \epsilon^{1/3})/\alpha$ . Conversely, in the low energy density limit,  $\epsilon \ll (G_0 \alpha)^{-3/2}$ , it reduces to  $H^2 + k/a^2 \simeq (8\pi G_0 \epsilon/3)(1 - \epsilon^{2/3}/\epsilon_{cr})$ , where  $\epsilon_{cr} = 5/(3\alpha G_0)$ .

- For the case with EOS  $w = 1$ , the Friedmann equation (72) is simplified to

$$H^2 + \frac{k}{a^2} = \frac{16\pi \sqrt{\epsilon}}{3\alpha} \left(1 - \frac{\ln(1 + \alpha G_0 \sqrt{\epsilon})}{\alpha G_0 \sqrt{\epsilon}}\right), \quad (76)$$

at high energy density, the above equation is simplified to  $H^2 + k/a^2 \simeq (16\pi \sqrt{\epsilon})/(3\alpha)$ , while in the low energy density limit,  $\epsilon \ll (G_0 \alpha)^{-2}$ , it takes the form  $H^2 + k/a^2 \simeq (8\pi G_0 \epsilon/3)(1 - \sqrt{\epsilon}/\epsilon_{cr})$ , where  $\epsilon_{cr} = 3/(2\alpha G_0)$ .

- For the case  $w = -1$ , the Friedmann equation (72) takes the following simple form

$$H^2 + \frac{k}{a^2} = \frac{8\pi G_0 \epsilon}{3}, \quad (77)$$

which gives  $\epsilon(a)|_{w=-1} = \epsilon_0$  according to Eq. (23). Thus, Eq. (77) describes the vacuum FLRW space time in the presence of the cosmological constant with  $\Lambda = 8\pi G_0 \epsilon_0$ .

- Another considerable case is  $|w| \gg 1$  which simplifies Eq. (72) to the following form

$$H^2 + \frac{k}{a^2} \simeq \frac{8\pi G_0 \epsilon}{3(1 + \alpha G_0 \epsilon^{\frac{1}{w}})} \simeq \frac{8\pi G_\infty \epsilon}{3} \left(1 - \frac{\alpha G_\infty \ln(\epsilon)}{w}\right), \quad (78)$$

In the limit  $w \rightarrow \pm\infty$ , Eq. (78) tends to the standard Friedmann equations

$$H^2 + \frac{k}{a^2} \simeq \frac{8\pi G_\infty \epsilon}{3}, \quad (79)$$

with a modified gravitational coupling constant.

### A. Stability

The modified equations outlined above can be extensively studied in cosmological contexts, especially in the early universe where the energy density is extremely high. Although the study of these equations is beyond the scope of this paper, additional calculations could provide deeper insights into them. It is instructive to express the field equations in terms of kinetic and potential energy [90], where the potential term can allow in a more detailed analysis of the system. The action given in Eq. (4) for the FLRW geometry can be written as  $S = \int \mathcal{L} d\tau$ , in which the Lagrangian is defined as follows

$$\mathcal{L} = \frac{-3V_3}{8\pi G_0} \left( a\dot{a}^2 - ka + \frac{a^3}{3} \chi(\epsilon)\epsilon \right), \quad (80)$$

where  $V_3$  is the volume of a three-dimensional space<sup>10</sup>. Defining the generalized momentum as  $p = \partial\mathcal{L}/\partial\dot{a} = -3V_3 a\dot{a}/4\pi G_0$  and constructing the Hamiltonian by performing a Legendre transformation on the lagrangian:  $\mathcal{H} = p\dot{a} - \mathcal{L}$ , we get

$$\mathcal{H} = -\frac{2\pi G_0}{3V_3} \frac{p^2}{a} - \frac{3V_3 a}{8\pi G_0} (V(a) + k), \quad (81)$$

we know that the  $G_{00}$  component of Einstein equations reduces to the condition on the Hamiltonian  $\mathcal{H} = 0$ . Thus, one can write

$$\dot{a}^2 + V(a) = -k, \quad (82)$$

this shows that our problem is equivalent to that of a particle with energy  $-k$  moving in the potential  $V(a)$ . The integral to be solved is

$$V(a) = -\frac{a^2}{3} \int_0^{\epsilon(a)} \frac{8\pi G_0}{1 + \alpha G_0 \epsilon^{\frac{1}{1+w}}} d\epsilon, \quad (83)$$

the solution of this integral involves the Hypergeometric function and can be expressed as

$$V(a) = -\frac{\Lambda_0}{3} a^2 - \frac{8\pi G_0 \epsilon_0}{3} a^{-3w-1} \times {}_2F_1 \left( 1, 1+w; 2+w; -\frac{\alpha G_0 \epsilon_0^{\frac{1}{1+w}}}{a^3} \right), \quad (84)$$

where the condition  $w > -1$  holds and  $\alpha, G_0 \in \mathbb{R}$ . Building upon Eq. (A5), we derive the asymptotic behavior of  $V(a)$  in the limits  $a \rightarrow 0$  and  $a \rightarrow \infty$ . A systematic analysis leads to the following result

$$\begin{cases} \lim_{a \rightarrow 0} V(a) \simeq -\frac{\Lambda_0}{3} a^2, & \text{if } w < -\frac{1}{3}, \\ \lim_{a \rightarrow \infty} V(a) \simeq -\frac{\Lambda_0}{3} a^2, & \text{if } w > -\frac{1}{3}, \end{cases} \quad (85)$$

<sup>10</sup> For a 4-dimensional space-time with three spatial dimensions, the volume of a three-dimensional space is given by  $V_3 = 4\pi \int_0^{r_b} r^2 / \sqrt{1 - kr^2} dr$ .

this result demonstrates that for a fluid with an equation of state parameter satisfying  $w < -\frac{1}{3}$ , the function  $V(a)$  follows a quadratic dependence for small scale factor. Conversely, for  $w > -\frac{1}{3}$ , the same quadratic form arises at large values. The symmetry in these asymptotic behaviors highlights the fundamental influence of  $w$  on the evolution of  $V(a)$  and suggests a direct connection between the dynamical properties of the system and the underlying equation of state.

By substituting Eq. (85) into Eq. (82), we obtain the following result

$$\left( \frac{\dot{a}}{a} \right)^2 + \frac{k}{a^2} \simeq \frac{\Lambda_0}{3}, \quad (86)$$

this equation represents the Friedmann equation in the presence of a cosmological constant  $\Lambda_0$ . The obtained expression corresponds to the vacuum solution of Einstein's field equations for the FLRW metric, where the energy density is dominated by the cosmological constant. In this scenario, the expansion of the system (universe) is governed solely by  $\Lambda_0$  and the curvature term  $k/a^2$ . For a spatially flat spacetime with  $k = 0$ , the scale factor in Eq. (86) evolves as  $a(t) \propto e^{\pm \sqrt{\Lambda_0/3} \tau}$ . Therefore, depending on the values of  $w$  at small and large distances, the scale factor exhibits exponential evolution. For the collapse process we know  $\dot{a} < 0$ , this implies  $R_b(\tau) = R_b(\tau_0) e^{-\sqrt{\Lambda_0/3} \tau}$ . So we have a fast decreasing radius at the small distances for equation of state with  $w < -1/3$ . We call this rapid decrease "deflation," inspired by the concept of early cosmic inflation. Such deflation has been shown in the gravitational collapse of an old star into a regular spacetime<sup>11</sup>.

In the following we derive the potential function (84) for specific values of  $w$ , and analyze its stability. In the following subsections we consider cosmological constant zero  $\Lambda_0 = 0$ .

#### 1. $w = 0$

In the case where the system behaves as dust, corresponding to  $w = 0$ , the potential function approaches

$$V(a) = -\frac{8\pi a^2}{3\alpha} \ln \left( 1 + \frac{\alpha G_0 \epsilon_0}{a^3} \right), \quad (87)$$

at large distances where  $a(\tau) \gg (\alpha G_0 \epsilon_0)^{1/3}$ , the potential function approaches  $V(a) \approx -G_0 \epsilon_0 / 3a$  which corre-

<sup>11</sup> It has been shown that the gravitational collapse of a star into Hayward spacetime predicts an exponential behavior for the star's radius at small distances, given by  $\tilde{R} \propto e^{-\tilde{\tau}/\tilde{l}}$  (see Ref. [18]). For Bardeen spacetime, the radius follows  $\tilde{R} \propto e^{-\tilde{\tau}/\tilde{g}^{3/2}}$  (see Ref. [18]), and for a spherically symmetric regular spacetime in asymptotically safe (AS) gravity, it is given by  $\tilde{R} \propto e^{-\tilde{\tau}/\tilde{A}}$  (see Ref. [19]).

sponds to the Newtonian gravitational potential. Conversely, for small values of the scale factor, the potential function in Eq. (87) takes the form  $V(a) \simeq (8\pi a^2/\alpha) \ln a$ . Assuming that the classical concept of the Newtonian force holds true in the small scale factor regime<sup>12</sup>, the force function can be expressed as  $F(a) \simeq -(16\pi a/\alpha) \ln a$ , indicating a repulsive force. However, this is not the complete picture. We can also express the force function corresponding to the potential derived in Eq. (87). Its behavior is illustrated in Fig. 8(b), where it is evident that at small distances ( $a < a_{\text{eq}}$ ), the force is repulsive, while at large distances ( $a > a_{\text{eq}}$ ), it becomes attractive.

The stability of a potential function is a critical aspect that describes the behavior of a system when subjected to small perturbations around its equilibrium points. To ascertain the stability of a potential function  $V(a)$ , it is essential to analyze both the first and second derivatives of the potential. The equilibrium points, denoted as  $a_{\text{eq}}$ , are determined by solving the equation  $V'(a) = 0$ . These points represent locations where the force, or equivalently the gradient of the potential, is zero.

To further assess the stability at these equilibrium points, we evaluate the second derivative of the potential,  $V''(a)$ . The sign of  $V''(a)$  at the equilibrium points provides insight into the stability of the system: if  $V''(a) > 0$ , the equilibrium point is stable, indicating that the system will return to equilibrium following a small perturbation; conversely, if  $V''(a) < 0$ , the equilibrium point is unstable, suggesting that perturbations will lead the system away from equilibrium.

The first derivative of the potential function  $V(a)$  is given by

$$V'(a) = \frac{8\pi G_0 \epsilon_0 a}{a^3 + \alpha G_0 \epsilon_0} - \frac{16\pi a \ln\left(1 + \frac{\alpha G_0 \epsilon_0}{a^3}\right)}{3\alpha}, \quad (88)$$

the second derivative of the potential function  $V(a)$  is

$$V''(a) = \frac{24\pi \alpha G_0^2 \epsilon_0^2}{(a^3 + \alpha G_0 \epsilon_0)^2} - \frac{16\pi \ln\left(1 + \frac{\alpha G_0 \epsilon_0}{a^3}\right)}{3\alpha}. \quad (89)$$

Dynamical stability often requires that the potential has local minima  $V_{\text{min}}$ , where particles can settle. At these minima, a small displacement causes a restoring force that drives the particle back to the equilibrium point. For a potential  $V(a)$  at an equilibrium point  $a_{\text{eq}}$ , stability generally requires that  $V''(a_{\text{eq}}) > 0$ . For the potential function given by Eq. (87), there is a minimum value  $V_{\text{min}}$  located at  $a_{\text{eq}}$ , as shown in Fig. 8(a). This figure illustrates the behavior of the potential function

as a function of the scale factor. The potential is negative for all values of the scale factor, starting at zero and rapidly decreasing to a minimum value before slowly increasing and asymptotically approaching zero at infinity. This behavior resembles the Newtonian gravitational potential  $V(a) \sim -G_0/a$ , which also tends to zero at large distances but diverges to negative infinity at small distances. Consequently, the potential function given by Eq. (87) corrects the Newtonian gravitational potential behavior at short distances.

The second derivative of the potential function (89) is shown in Fig. 8(c). It demonstrates that for  $a_1 < a < a_2$ , the second derivative is positive, indicating that the potential function can be stable in this range. The equilibrium point  $a_{\text{eq}}$  lies within this interval, meaning that the system has a dynamically stable potential given by Eq. (87), with its minimum value located at  $a_{\text{eq}}$ . We can also examine the behavior of the scale factor near the equilibrium point  $a_{\text{eq}}$ . To do this, we substitute  $V_{\text{min}}$  into Eq. (82), which yields the following result

$$\dot{a} = \pm \sqrt{-V_{\text{min}} - k} \Rightarrow a(\tau) = \gamma\tau, \quad (90)$$

where  $\gamma = \sqrt{-V_{\text{min}} - k}$ . In Eq. (87), it is evident that the minimum value of the potential depends on certain integration constants that have emerged during the calculations. Specifically, we can express this minimum as  $V_{\text{min}} = V(G_0, \alpha, \epsilon_0, a_{\text{eq}})$ . Consequently, the potential can vary with different values of these constants. However, to ensure a physically acceptable prediction, the condition  $V_{\text{min}} + k < 0$  must be satisfied. This requirement is essential for the scale factor to remain real.

We want to evaluate the stable point more, by considering the small displacement around  $a_{\text{eq}}$ . The potential expansion is given by  $V(a) \simeq V(a_{\text{eq}}) + [V''(a_{\text{eq}})/2](a - a_{\text{eq}})^2$ . Substituting this into Eq. (90) gives the following integration

$$\tau - \tau_0 = \int \frac{dy}{\gamma \sqrt{1 - (b/2\gamma^2)y^2}}, \quad y = a - a_{\text{eq}}, \quad (91)$$

where  $b = V''(a_{\text{eq}})$ . The solution of the above integral for star's surface is given by

$$R_b(\tau) = r_b a_{\text{eq}} + r_b \gamma \sqrt{\frac{2}{b}} \sin\left(\sqrt{\frac{b}{2}} \tau\right), \quad (92)$$

For a short time period  $\tau \ll 1$ , Eq. (92) approximates to  $R_b(\tau) \simeq r_b a_{\text{eq}} + r_b \gamma \tau$ . The behavior of Eq. (92) is shown in Fig. 9. It oscillates around the equilibrium point  $a_{\text{eq}}$ . The oscillation of a star's surface radius around the equilibrium point can be an intriguing subject for both theoretical and observational physics.

<sup>12</sup> It is clear that the accuracy of the classical notion of gravity, expressed as the gradient of the gravitational potential,  $F(a) = -\partial V(a)/\partial a$ , has not been empirically tested at small distances. Here, we use it to evaluate and compare the given potential function to gain a deeper insight into its evolution.

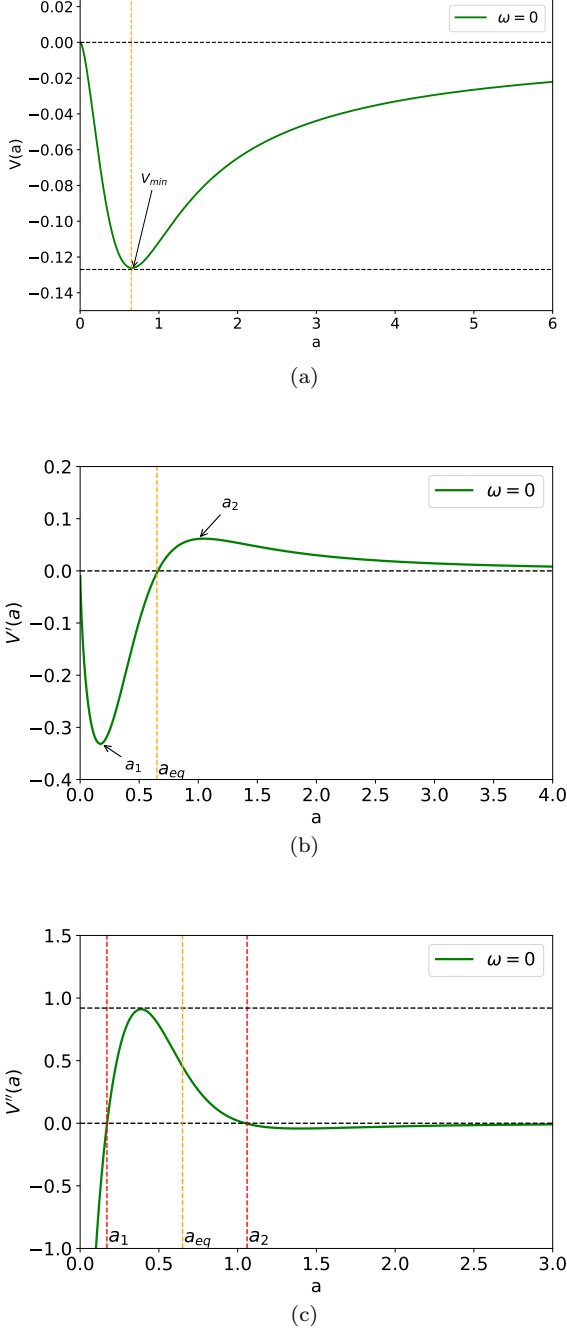


FIG. 8. The potential function Eq. (87), its first derivative Eq. (88), and its second derivative Eq. (89) are shown as a function of the scale factor  $a$ . The parameters are set to  $\epsilon_0 = 5/4\pi$ ,  $\alpha = 8\pi$ ,  $G_0 = 1/8\pi$ .

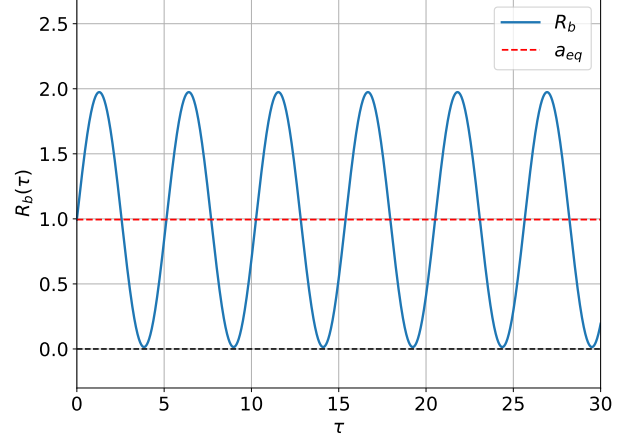


FIG. 9. The star's radius  $R_b(\tau)$  according to Eq. (92) with  $\gamma = 1.2$ , and  $b = 3$ .

## 2. $w = -1/2$

For a system consisting of exotic matter with  $w = -1/2$ , the potential function takes the form

$$V(a) = -\frac{8\pi}{3} \sqrt{\frac{G_0}{\alpha}} a^2 \arctan\left(\frac{\epsilon_0 \sqrt{\alpha G_0}}{a^{3/2}}\right), \quad (93)$$

At small distances, the potential function in Eq. (93) simplifies to  $V(a) = -Ca^2/3$ , where  $C = 4\pi^2 \sqrt{G_0/\alpha}$ . This expression matches the potential function of de Sitter spacetime. Applying the classical definition of force to this potential yields  $F(a) \sim Ca$ , indicating a repulsive force. At large distances, the potential function approaches  $V(a) \sim -(8\pi G_0 \epsilon_0/3) \sqrt{a}$ , leading to a repulsive force given by  $F(a) \sim (4\pi G_0 \epsilon_0/3)/\sqrt{a}$ . The potential in Eq. (93) exhibits an intriguing property: its derivative, interpreted as a classical force, remains repulsive and displays distinct behaviors at different distances. At large distances, the force decreases inversely with the square root of the distance, whereas at small distances, it varies linearly with distance.

To analyze the dynamics and stability of the potential in Eq. (93), we must compute its first and second derivatives, as previously stated. The first derivative is expressed as

$$V'(a) = -\frac{16\pi a}{3} \sqrt{\frac{G_0}{\alpha}} \arctan\left(\frac{\epsilon_0 \sqrt{G_0 \alpha}}{a^{3/2}}\right) + \frac{4\pi \epsilon_0 G_0}{a^3 + \alpha G_0 \epsilon_0^2} a^{5/2}, \quad (94)$$

the second derivative can also be expressed as

$$V''(a) = -\frac{16\pi}{3}\sqrt{\frac{G_0}{\alpha}}\arctan\left(\frac{\epsilon_0\sqrt{G_0\alpha}}{a^{3/2}}\right) + \frac{18\pi\epsilon_0 G_0}{a^3 + \alpha G_0 \epsilon_0^2}a^{3/2} - \frac{12\pi G_0 \epsilon_0 a^{9/2}}{(a^3 + \alpha G_0 \epsilon_0^2)^2}, \quad (95)$$

the potential function defined by Eq. (93) does not exhibit a local minimum, as demonstrated in Fig. 10(a). It decreases monotonically with a decreasing scale factor  $a$ , indicating the absence of a stable equilibrium in the traditional sense, meaning there is no local minimum of the potential. However, at  $a = 0$ , both the potential function and its derivative, as described by Eq. (94), reach zero, as shown in Fig. 10(b). Nevertheless, the second derivative, presented in Eq. (95) and depicted in Fig. 10(c), is negative, indicating that the potential is unstable at  $a = 0$ . Thus, the potential lacks a minimum value and is unstable, in contrast to the potential function for  $w = 0$ .

$$3. \quad w = \frac{1}{2}$$

For a system consisting of an equation of state with  $w = 1/2$ , the potential function (83) takes the form

$$V(a) = \frac{8\pi a^2}{\alpha\sqrt{\alpha G_0}}\arctan\left(\frac{\epsilon_0^{1/3}\sqrt{\alpha G_0}}{a^{3/2}}\right) - \frac{8\pi\epsilon_0^{1/3}}{\alpha}a^{1/2}, \quad (96)$$

at large distances ( $a \rightarrow \infty$ ), the potential function behaves asymptotically as  $V(a) \simeq -8\pi\epsilon_0 G_0/3a^{5/2}$ . This result indicates that the potential approaches zero from the negative side, following an inverse power-law decay with respect to  $a$ . The associated force function is given by  $F(a) \simeq -20\pi\epsilon_0 G_0/3a^{7/2}$ . Since this force is negative, it acts as an attractive force, meaning it pulls objects toward smaller values of  $a$ . The power-law dependence ( $a^{-7/2}$ ) implies that the attractive force rapidly weakens as  $a$  increases, leading to a diminishing effect at very large distances. In contrast, at small distances ( $a \rightarrow 0$ ), the potential takes a different asymptotic form:  $V(a) \simeq -8\pi\epsilon_0^{1/3}\sqrt{a}/\alpha$ . Unlike the large-distance case, this expression exhibits a square-root dependence on  $a$ , indicating a much slower variation of the potential near  $a = 0$ . The corresponding force function, obtained by differentiating the potential, is  $F(a) \simeq 4\pi\epsilon_0^{1/3}/\alpha\sqrt{a}$ . This force is positive, meaning it remains repulsive. However, in this regime, the force diverges as  $a \rightarrow 0$ , implying that as the system approaches very small distances, the repulsive interaction becomes extremely strong. This suggests a dominant influence of the potential at small scales, potentially preventing the system from reaching  $a = 0$  due to an infinitely increasing repulsive force.

To examine the dynamics and stability of the potential given in Eq. (93), we need to calculate its first and second derivatives, as mentioned earlier. The first derivative can

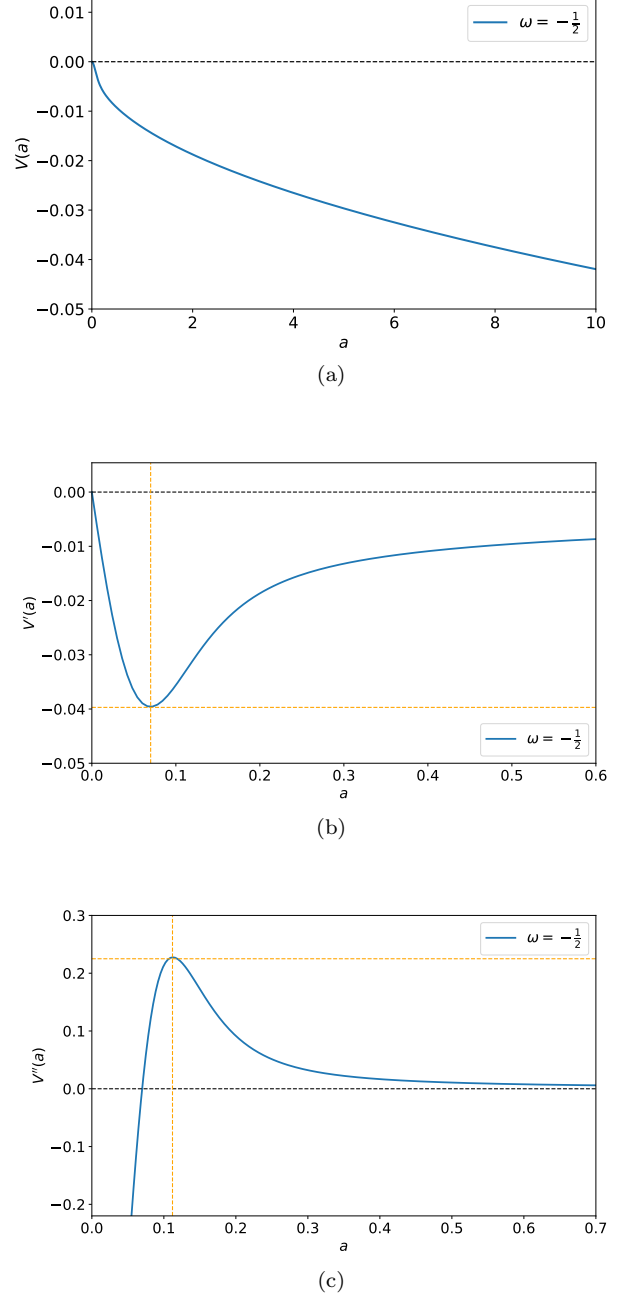


FIG. 10. The potential function (93), its first derivative Eq. (94), and its second derivative Eq. (95) as a function of the scale factor  $a$ . The parameters are set as  $\alpha = 8\pi$ ,  $\epsilon_0 = G_0 = 1/8\pi$ .

be expressed as follows

$$V'(a) = -\frac{4\pi\epsilon_0^{1/3}}{\alpha\sqrt{a}} - \frac{12\pi\epsilon_0^{1/3}}{\alpha}\frac{a^{5/2}}{a^3 + \alpha G_0 \epsilon_0^{2/3}} + \frac{16\pi a}{\alpha\sqrt{\alpha G_0}}\arctan\left(\frac{\sqrt{\alpha G_0}\epsilon_0^{1/3}}{a^{3/2}}\right), \quad (97)$$

and second derivatives of the potential function is given by

$$V''(a) = \frac{-16\pi a^6 \epsilon_0^{1/3} - 50\pi a^3 \alpha G_0 \epsilon_0 + 2\pi \alpha^2 G_0^2 \epsilon_0^{5/3}}{a^{3/2} \alpha (a^3 + \alpha G_0 \epsilon_0^{2/3})^2} + \frac{16\pi G_0 \arctan\left(\frac{\sqrt{\alpha G_0 \epsilon_0^{1/3}}}{a^{3/2}}\right)}{(\alpha G_0)^{3/2}}. \quad (98)$$

The potential function given by Eq. (96) has a minimum value,  $V_{\min}$ , at  $a_{\text{eq}}$ , as shown in Fig. 11(a), which illustrates how the potential changes with the scale factor. The second derivative of the potential, described by Eq. (98), is plotted in Fig. 11(c). This plot shows that for  $a < a_c$ , the second derivative is positive, suggesting that the potential is stable in this range. Since the equilibrium point  $a_{\text{eq}}$  falls within this region, the system remains dynamically stable.

#### 4. $w = 1$

For a system containing matter with  $w = 1$ , the potential function (84) is given by

$$V(a) = \frac{16\pi a^2}{3\alpha^2 G_0} \ln\left(1 + \frac{\alpha G_0 \sqrt{\epsilon_0}}{a^3}\right) - \frac{16\pi \sqrt{\epsilon_0}}{3\alpha a}, \quad (99)$$

at large distances, the potential function  $V(a)$  asymptotically approaches  $V(a) \simeq -8\pi G_0 \epsilon_0 / (3\alpha a^4)$ . The corresponding force function is given by  $F(a) \simeq -32\pi G_0 \epsilon_0 / (3\alpha a^5)$ . This force is attractive, as indicated by its negative sign, and exhibits an inverse power-law dependence on the scale factor  $a$ . The steep falloff with increasing  $a$  suggests that the interaction weakens significantly at large distances. Conversely, in the limit of small distances ( $a \rightarrow 0$ ), the potential is dominated by the term  $V(a) \simeq -16\pi \sqrt{\epsilon_0} / (3\alpha a)$ . The force associated with this potential is  $F(a) \simeq -16\pi \sqrt{\epsilon_0} / (3\alpha a^2)$ . This force exhibits a divergence as  $a \rightarrow 0$ , implying an increasingly strong attractive interaction at small distances. The  $a^{-2}$  dependence suggests a resemblance to gravitational or Coulomb-like behavior, where the force becomes significantly stronger as the separation decreases. This divergence highlights the presence of a dominant short-range interaction that governs the system at sufficiently small scales.

To analyze the dynamics and stability of the potential in Eq. (99), it is essential to determine its first and second derivatives. As previously stated, the first derivative is given by

$$V'(a) = \frac{32\pi a}{3\alpha^2 G_0} \ln\left(1 + \frac{\alpha G_0 \sqrt{\epsilon_0}}{a^3}\right) + \frac{16\pi \sqrt{\epsilon_0}}{3\alpha a^2} - \frac{16\pi \sqrt{\epsilon_0}}{\alpha} \frac{a}{a^3 + \alpha G_0 \sqrt{\epsilon_0}}, \quad (100)$$

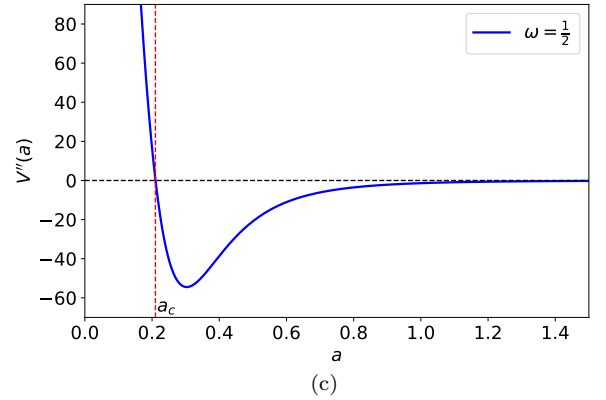
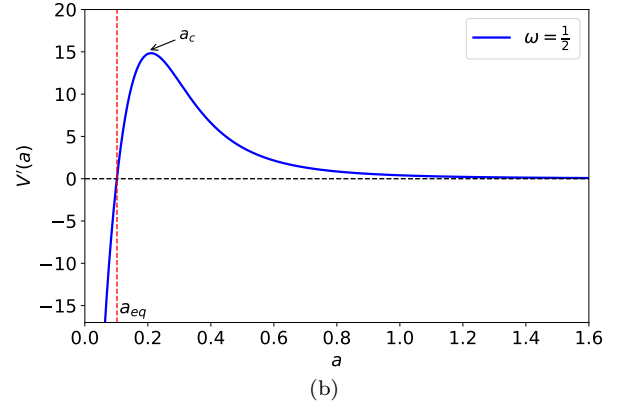
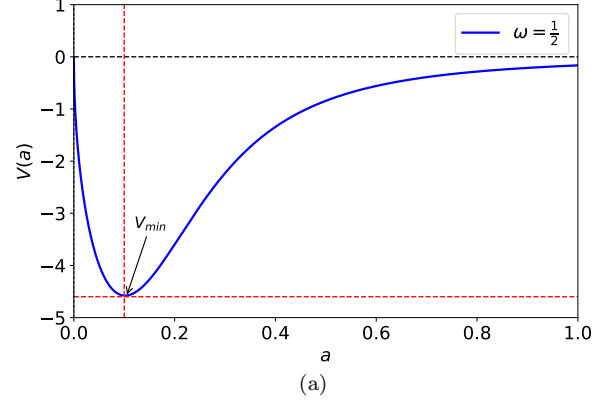


FIG. 11. The potential function (96), its first derivative Eq. (97), and its second derivative Eq. (98) as a function of the scale factor  $a$ . The parameters are set as  $\alpha = 1$ ,  $\epsilon_0 = 0.5$ ,  $G_0 = 1/8\pi$ .

the second derivative is likewise given by

$$V''(a) = -\frac{32\pi \sqrt{\epsilon_0}}{3\alpha a^3} - \frac{48\pi G_0 \epsilon_0}{(a^3 + \alpha G_0 \sqrt{\epsilon_0})^2} + \frac{32\pi}{3\alpha^2 G_0} \ln\left(1 + \frac{G_0 \alpha \sqrt{\epsilon_0}}{a^3}\right), \quad (101)$$

It was stated that for stability, an equilibrium point  $a_{\text{eq}}$  must satisfy  $V'(a_{\text{eq}}) = 0$ . However, Fig. 12(a) and Fig. 12(b) demonstrate that  $V'(a_{\text{eq}}) \neq 0$  for any finite  $a$ , indicating the absence of a stable equilibrium. Furthermore, Fig. 12(c) shows that  $V''(a_{\text{eq}}) < 0$ , meaning the potential is concave down, which also does not support stability. Therefore, the potential equation (99) is not dynamically stable.

The above analysis shows that there are both dynamically stable and unstable potential functions for different values of  $w$ . We have chosen some values  $w \in \{-1/2, 0, 1/2, 1\}$ , but it is also possible to find other potential functions for different equations of state. In the following, we will attempt to study the exterior region of the gravitationally collapsing object and its properties as it evolves into a BH.

#### IV. BLACK HOLE SOLUTIONS

It is well known that there is insufficient information about the EOS that governs the final state of gravitationally collapsed objects. The polytropic EOS could be a possible choice to describe the gravitational collapse process leading to a regular BH in the final stage of collapse [18]. Some known gravitational theories also predict complex EOS that tend to  $w = -1/2$  for collapsing stars at high energy densities [20]. In this section, we will consider the EOS in the range  $-1 \leq w \leq 1$ , which is widely recognized in cosmology and encompasses both ordinary matter and quintessence.

In the previous sections, we extensively studied the dynamics of both the interior and the surface of the star, as well as the junction conditions connecting its interior and exterior. Our goal now is to evaluate the physics governing the region outside the star. On the surface of the star, comparing Eq. (21) and Eq. (72) gives the MS mass  $m(R)$  as follows

$$m_w(R) = \frac{\zeta_w}{R^{3w}} {}_2F_1\left(1, 1+w; 2+w; -\frac{\rho G_0}{R^3}\right), \quad (102)$$

where  $\zeta_w = 4\pi G_0 \epsilon_0 r_b^{3(1+w)}/3$ . The MS mass function (102) is the primary prediction of our theory. It encapsulates all the information about the curvature of the given spacetime and the evolution of the region outside the star. Its behavior as a function of radial distance for different EOS is shown in Fig. 14, Fig. 15, and Fig. 16. Furthermore, the behavior of  $m_w(R)$  is depicted as a contour plot in Fig. 13. This motivates us to examine specific values of  $w$  to assess the dynamics outside the star.

##### 1. $w = 0$

For dust gravitational collapse,  $w = 0$ , the MS mass Eq. (102) is simplified to

$$m_0(R) = \frac{R^3}{6\xi} \ln\left(1 + \frac{6m_0 G_0 \xi}{R^3}\right), \quad (103)$$

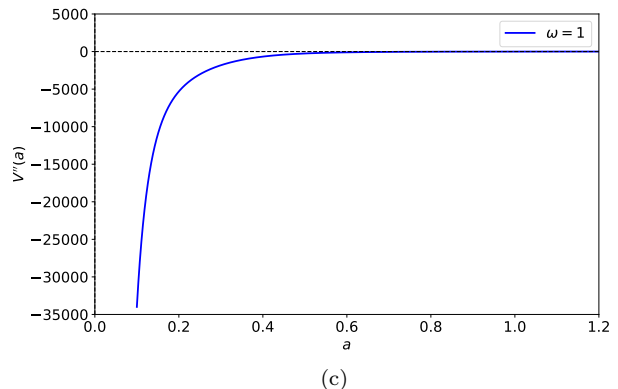
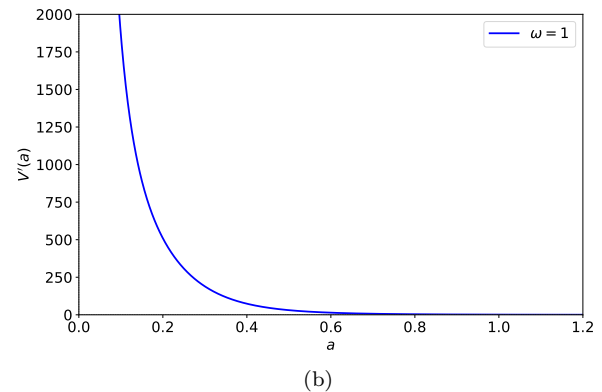
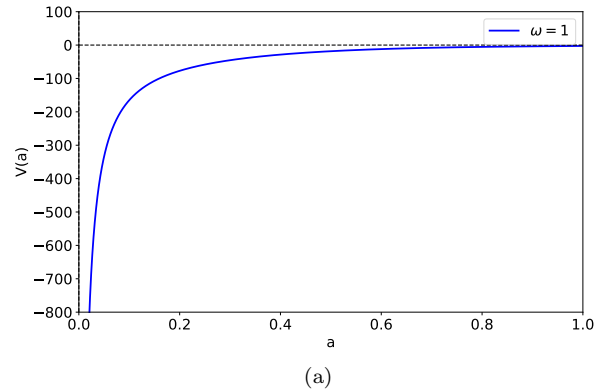


FIG. 12. The potential function (99), its first Eq. (100), and second Eq. (101) derivatives are shown as function of the scale factor  $a$ . The parameters are set as  $\epsilon_0 = \alpha = 1$ ,  $G_0 = 1/8\pi$ .

where  $\xi = 3\beta^2/8g_*m_0$ , and the initial comoving energy density was assumed to be  $\epsilon_0 = 3m_0/4\pi r_b^3$ . The MS mass Eq. (103) is recently derived for a dust fluid in Ref. [64], where the interior matter is modeled as a dust fluid with  $w = 0$ . The corresponding metric function is given by

$$f(R) = 1 - \frac{R^2}{3\xi} \ln\left(1 + \frac{6m_0 G_0 \xi}{R^3}\right). \quad (104)$$

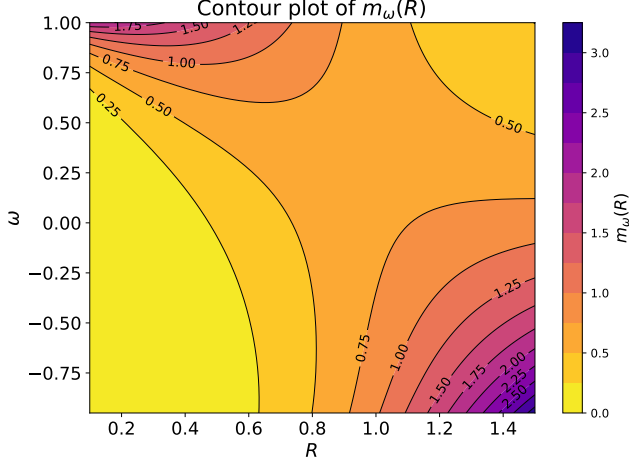


FIG. 13. Contour plot of the MS mass function (102) for  $R \in [0.1, 1.5]$  and  $w \in (-0.95, 1]$ . The plot reveals how  $m_w(R)$  varies with both parameters. The contours highlight regions of rapid change and indicate how the mass function behaves across different scales. The parameter values are set to  $\zeta = G_0 = \varrho = 1$

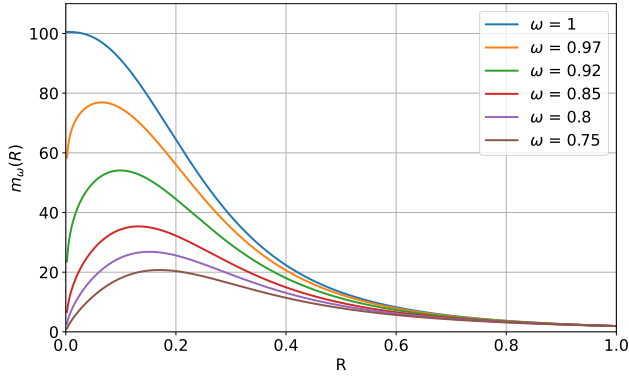


FIG. 14. The MS mass function (102) for some positive values of  $w \in [0.75, 1]$ . At large distances, the MS mass tends to zero regardless of the values of  $w$ , while at small distances, the rate of its changes and its maximum value vary with  $w$ . The parameters are set as  $\epsilon_0 = \alpha = 1, G_0 = 1/8\pi$ .

At large distances, where  $R^3 \gg 6m_0G_0\xi$ , Eq. (103) becomes  $f(R) \simeq 1 - 2m_0G_0/R$ , which corresponds to the Schwarzschild metric component. To determine the event horizon, we examine Eq. (104) for  $f(R) = 0$ . While it is not possible to obtain an exact analytical solution, nu-

merical methods provide a simple and effective way to find the solutions. The behavior of  $f(R)$  as a function of radial distance is shown in Fig. 17. This figure illustrates that the roots of  $f(R)$  are strongly dependent on the values of  $\xi$ . For  $\xi = 1$ , there is no horizon; for  $\xi = 0.29$ , there is a single event horizon; and for  $\xi = 0.05$ , there are

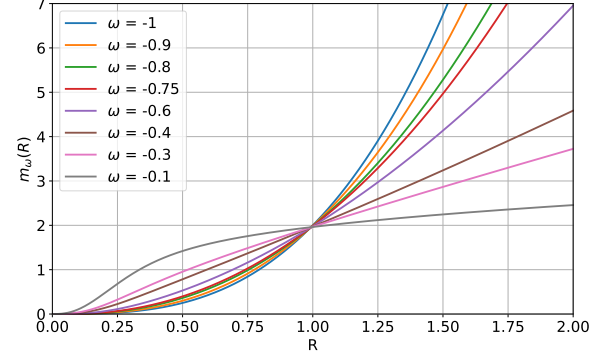


FIG. 15. The MS mass function (102) for some negative values of  $w \in [-0.1, -1]$ . The MS mass function increases with radius and approaches zero at small distances. The parameters are set as  $\varrho = \zeta_w = 1, 8\pi G_0 = 1$ .

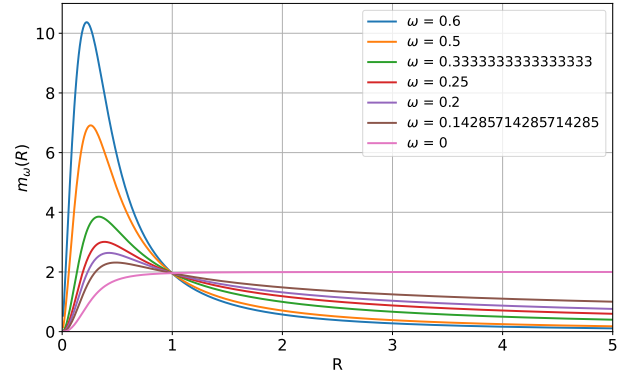


FIG. 16. The MS mass function (102) for selected positive values of  $w \in [0, 0.6]$ . At large distances, the MS mass approaches zero regardless of  $w$ , while at small distances, both its rate of change and maximum value depend on  $w$ . The parameters are set as  $\varrho = \zeta_w = 1, 8\pi G_0 = 1$ .

two horizons. To investigate the divergence of the metric at the center of a BH, where  $R \rightarrow 0$ , one can calculate the Kretschmann scalar for the specified metric given in Eq. (104). It is expressed as

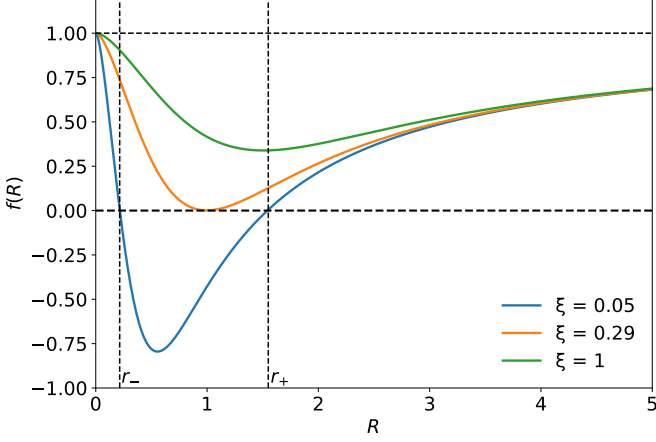


FIG. 17. The behavior of  $f(R)$  as a function of radial distance  $R$  according to (104), for values  $\xi = \{0.05, 0.29, 1\}$ ,  $m_0 = 20$ , and  $8\pi G_0 = 1$ . The horizons are denoted by  $r_-$  and  $r_+$ .

$$\begin{aligned}
K(R) = & \frac{4}{\xi^2} \left( \ln \left( 1 + \frac{b}{R^3} \right) - \frac{b}{2(R^3 + b)^2} \right)^2 + \frac{8}{\xi^2} \left( \ln \left( 1 + \frac{b}{R^3} \right) - \frac{b}{R^3 + b} \right)^2 + \frac{4}{3\xi^2} \left( \ln \left( 1 + \frac{b}{R^3} \right) \right)^2 \\
& - \frac{16}{3\xi^2} \left( \ln \left( 1 + \frac{b}{R^3} \right) - \frac{3b}{2(R^3 + b)} \right) \left( \ln \left( 1 + \frac{b}{R^3} \right) - \frac{5b^2 + 2bR^3}{2(R^3 + b)^2} \right) \\
& - \frac{16}{3\xi^2} \left( \ln \left( 1 + \frac{b}{R^3} \right) - \frac{b}{R^3 + b} \right) \ln \left( 1 + \frac{b}{R^3} \right), \tag{105}
\end{aligned}$$

where  $b = 6m_0G_0\xi$ . At large radial distances, where  $R^3 \gg b$ , the Kretschmann scalar approximates to  $K(R) \simeq 48G_0m_0/R^6$ . This expression represents the Kretschmann scalar derived from the Schwarzschild metric. However, at small radial distances, where  $R^3 \ll b$ , the situation changes, and the Kretschmann scalar can be expressed as

$$K(R) \simeq \frac{24}{\xi^2} (\ln R)^2, \tag{106}$$

at the center of the BH, as  $R \rightarrow 0$ , a singularity occurs where  $K(R) \rightarrow \infty$ . Nevertheless, this is a mathematical singularity, and under specific physical conditions, it may be feasible to impose a cutoff at small distances, ensuring that  $R > R_{\min}$ . In this scenario, the curvature remains finite, as discussed in Ref. [64].

## 2. $w = -1$

A significant value of the EOS parameter is  $w = -1$ , which is widely recognized in cosmological physics and alternative BH models, such as gravastars (gravitational vacuum condensate stars) [96]. In this case, Eq. (102)

simplifies to

$$m_{-1}(R) = \zeta_{-1}R^3, \tag{107}$$

this mass term corresponds exactly to de Sitter spacetime, where  $f(R)|_{w=-1} = 1 - \Lambda R^2/3$ , with the cosmological constant  $\Lambda = 8\pi G_0\epsilon_0$ . The properties and implications of this spacetime have been extensively studied and are well established in gravitational and high-energy physics.

## 3. $w = -1/2$

For  $w = -1/2$ , the mass function given in Eq. (102) simplifies to

$$m_{-\frac{1}{2}}(R) = \eta R^3 \arctan \left( \sqrt{\frac{G_0 \rho}{R^3}} \right), \tag{108}$$

where the constant  $\eta$  is defined as  $\eta = 8\pi\epsilon_0\sqrt{G_0g_*r_b^3}/9\beta$ . To derive Eq. (108), we have employed Eq. (A11), which establishes the relation between the hypergeometric function and the inverse tangent function. The corresponding

metric function associated with this mass term is given by

$$f(R) = 1 - 2\eta R^2 \arctan\left(\sqrt{\frac{G_0 \varrho}{R^3}}\right). \quad (109)$$

Notably, the presence of the arctan function in  $f(R)$  suggests a deviation from a simple power-law correction, indicating a nontrivial gravitational modification in this regime. The behavior of the metric function for large and small  $R$  can provide insights into the asymptotic structure of the solution, potentially revealing distinct gravitational signatures in comparison to standard cases. At large distances, where  $R$  is sufficiently large, the metric function asymptotically behaves as

$$f(R) \simeq 1 - 2\eta\sqrt{G_0\varrho}\sqrt{R}. \quad (110)$$

On the other hand, in the small-distance regime where  $R^3 \ll G_0\varrho$ , the metric function simplifies to

$$f(R) \simeq 1 - \pi\eta R^2, \quad (111)$$

this expression corresponds to a de Sitter-like space-time, characterized by an effective cosmological constant. The emergence of a quadratic dependence on  $R$  at short distances indicates a dominant repulsive effect, resembling an inflationary or dark energy-like behavior.

To determine the event horizon, we analyze the equation  $f(R) = 0$  for Eq. (109). Although an exact analytical solution is not feasible, the solutions can be easily demonstrated using numerical methods. Fig. 18 shows that the

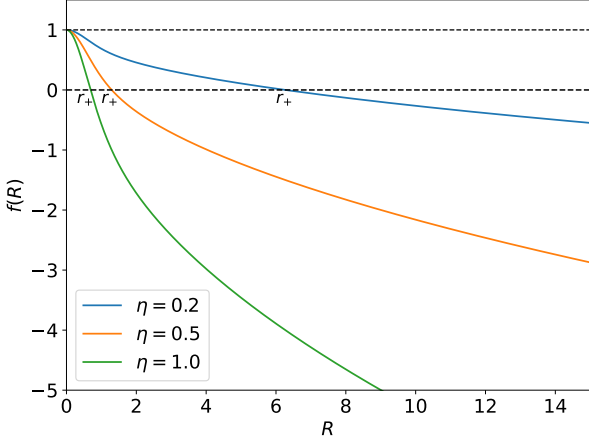


FIG. 18. The behavior of  $f(R)$  as a function of the radial distance  $R$  for different values of  $\eta$  and  $G_0\varrho = 1$ , according to Eq. (109). The plot shows that there is a single event horizon  $r_+$ .

spherically symmetric metric Eq. (109) possesses a single horizon, indicating the presence of a BH in this space-time. To explore the presence of a singularity in this spacetime, we should compute curvature scalars, such as

the Kretschmann scalar. As mentioned, at small distances the metric function becomes the de-sitter space-time  $f(R) \simeq 1 - \pi\eta R^2$ , and the Kretschmann scalar becomes  $K(R) \simeq \pi^2\eta^2$ . Therefore, space-time given with Eq. (109) is regular at  $R \rightarrow 0$ .

#### 4. $w = 1$

Now, let us consider an another equation of state with  $w = 1$ . Substituting this into Eq. (102) yields the following expression for the MS mass equation as

$$m_1(R) = \frac{2\zeta_1}{\varrho G_0} - \frac{2\zeta_1 R^3}{(\varrho G_0)^2} \ln\left(1 + \frac{\varrho G_0}{R^3}\right), \quad (112)$$

the metric function corresponding to this mass function is given by

$$f(R) = 1 - \frac{2M}{R} + \frac{2M}{\varrho G_0} R^2 \ln\left(1 + \frac{\varrho G_0}{R^3}\right), \quad (113)$$

where  $M = 2\zeta_1/(\varrho G_0)$ . For large distances  $R \gg (G_0\varrho)^{1/3}$ , the metric function (113) becomes

$$f(R) \simeq 1 - \frac{M\varrho G_0}{R^4}. \quad (114)$$

The presence of a term proportional to  $R^{-4}$  in the spherically symmetric space-time metric has been explored in several prominent theories of quantum gravity, including loop quantum gravity [21, 99, 100] and quantum modified gravity theories [101].

At small distances  $R \rightarrow 0$ , the metric function (113) becomes

$$f(R) \simeq 1 - \frac{2M}{R} - \frac{2M \ln(\varrho G_0)}{\varrho G_0} R^2 - \frac{6M}{\varrho G_0} R^2 \ln R, \quad (115)$$

which corresponds to the Schwarzschild–de Sitter metric modified by the presence of a logarithmic term.

The computation of the Kretschmann scalar confirms the existence of a singularity as  $R \rightarrow 0$  within this metric. Additionally, the behavior of the metric function  $f(R)$  in relation to  $R$  is depicted in Fig. 19. The figure illustrates that there is only one finite value of  $R$  at which the metric component  $f(R)$  vanishes, indicating the presence of a single event horizon for this BH.

#### 5. $w = 1/2$

Choosing the equation of state  $w = 1/2$ , the MS mass term Eq. (102) becomes

$$m_{1/2}(R) = 3\Upsilon R^{3/2} \left(1 - \frac{\arctan(\sqrt{\rho G_0} R^{-3/2})}{\sqrt{\rho G_0} R^{-3/2}}\right), \quad (116)$$

where  $\Upsilon = \zeta_{1/2}/(\rho G_0)$ . The metric function for the above mass function is written as

$$f(R) = 1 - 6\Upsilon\sqrt{R} \left(1 - \frac{\arctan(\sqrt{\rho G_0} R^{-3/2})}{\sqrt{\rho G_0} R^{-3/2}}\right), \quad (117)$$

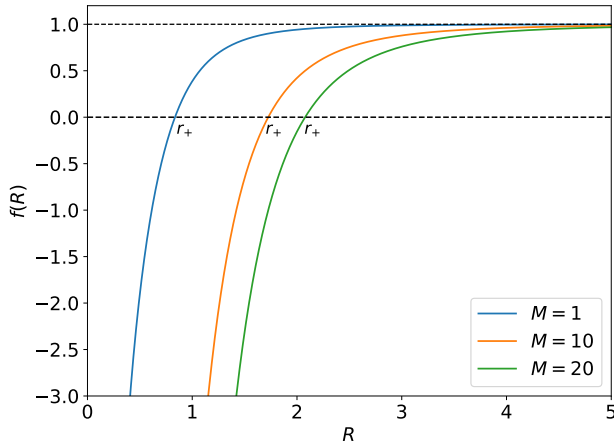
6.  $|w| \gg 1$ 

FIG. 19. Behavior of the metric function (113) with respect to the radial distance  $R$  for  $\varrho G_0 = 1$ . The plot shows that there is a single event horizon  $r_+$ .

for small distances  $R^3 \ll G_0 \varrho$ , the metric function (117) is given  $f(R) \simeq 1 - 6\Upsilon\sqrt{R}$ . For  $R \gg G_0 \varrho$ , the metric component would be  $f(R)|_{w=1/2} \simeq 1 - q^2/R^{5/2}$ , where  $q = \sqrt{2\zeta_{1/2}}$ .

By calculating the Kretschmann scalar, we verify that a singularity emerges as  $R \rightarrow 0$  in this metric. Furthermore, Fig. 20 presents how the metric function  $f(R)$  varies with  $R$ . As shown in the figure,  $f(R)$  reaches zero at two finite values of  $R$ , revealing that this BH has two horizons, inner horizon  $r_-$ , and outer horizon  $r_+$ .

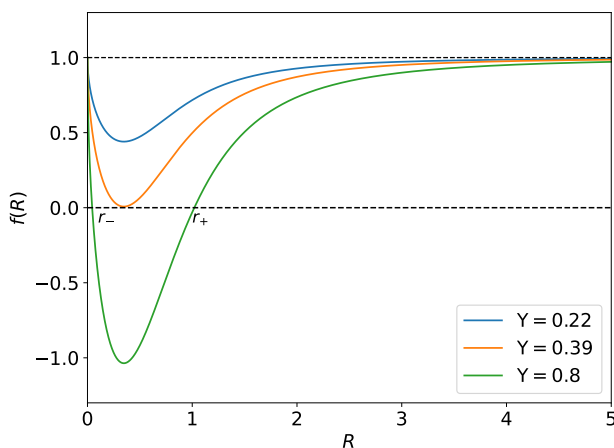


FIG. 20. Behavior of the metric component  $f(R)$  as a function of the radial distance  $R$  for the values  $\Upsilon = \{0.22, 0.39, 0.8\}$  and  $G_0 \rho = 1$ .

In this case, the MS mass term Eq. (102) is given by

$$m_w(R) \simeq \frac{\xi_w}{R^{3w}} \frac{1}{R^3 + \varrho G_0}, \quad (118)$$

the metric function corresponding to the given mass function is expressed as

$$f(R) \simeq 1 - 2\xi_w \frac{R^{-3w}}{R^3 + \varrho G_0}. \quad (119)$$

For positive values of  $w$ , where  $|w| = w$ , the metric function in Eq. (119) develops a singularity as  $R \rightarrow 0$ . On the other hand, when  $|w| = -w$  (negative values), the spacetime remains well-behaved. This is evident from the Kretschmann scalar, which follows  $K(R) \propto m_w(R)$ . Since the MS mass term remains finite in the limit  $w \ll -1$  and  $R \rightarrow 0$ , the spacetime remains regular in this case.

## 7. Kiselev-Like Black Hole

In general, according to the power series (A5), at large distances  $R \gg (G_0 \varrho)^{1/3}$  the equation (102) reduces to  $m_w(R) \simeq \zeta_w/R^{3w}$ , and the space-time metric is given by

$$ds^2 = - \left(1 - \frac{2\zeta_w}{R^{1+3w}}\right) dt^2 + \left(1 - \frac{2\zeta_w}{R^{1+3w}}\right)^{-1} dR^2 + R^2 d\Omega^2, \quad (120)$$

the above metric is the Kiselev BH [87], with zero schwarzschild mass,  $m = 0$ , and  $K = 2\zeta_m$ . It is well known that the Kiselev metric is the static spherically symmetric solution of Einstein's equations whose source is a non-perfect fluid with anisotropic pressures [102]. It has been demonstrated that the Kiselev metric reduces to the Reissner–Nordström metric when the averaged equation of state satisfies  $w = 1/3$  [103]<sup>13</sup>. We have shown above that the Kiselev metric can also be a solution of AS gravity at large distances whose source is a perfect fluid with a linear equation of state (but in the presence of running gravitational coupling and running cosmological constant). From another point of view, if we take into account the equations of AS gravity with the effective energy momentum tensor Eq. (25), then the source of the

<sup>13</sup> The metric of the Kiselev BH is given by

$$ds^2 = - \left(1 - \frac{2m}{R} - \frac{K}{R^{1+3w}}\right) dt^2 + \frac{dR^2}{1 - \frac{2m}{R} - \frac{K}{R^{1+3w}}} + R^2 d\Omega^2, \quad (121)$$

where  $m$  is the schwarzschild mass. For  $\omega = 1/3$  and  $K = -Q^2$ , this metric simplifies to the Reissner–Nordström metric, and the average pressure satisfies the radiation equation of state  $\bar{p} = (p^R + p^\theta + p^\phi)/3 = \rho/3$  (see Ref. [103]).

Kiselev metric is a fluid with anisotropic pressures, unless  $m''(R) = 2m'(R)/R$  which gives the Schwarzschild de Sitter BH with the mass function  $m(R) = AR^3/3 + B$ . By substituting the metric from Eq. (120) into Eq. (26), and considering the average tangential and radial pressures, we can express the equation of state as the ratio of the average pressure to the density. Consequently, the equation of state takes on a linear form, as shown below

$$\bar{p}_e = \frac{p_e^R + p_e^\theta + p_e^\phi}{3} = -\frac{3w^2\xi_w}{4\pi R^{3(w+1)}}; \quad \frac{\bar{p}_e}{\rho_e} = w, \quad (122)$$

for the general mass function (102), the ratio of the average pressure to the density would be

$$w(R) = \frac{\bar{p}_e}{\rho_e} = \frac{9w^2\alpha(R) - 3(2w+1)\beta(R) + \gamma(R)}{3(3w\alpha(R) - \beta(R))}, \quad (123)$$

where

$$\begin{aligned} \alpha(R) &= {}_2F_1\left(1, 1+w; 2+w; -\frac{G_0\rho}{R^3}\right), \\ \beta(R) &= \frac{3\rho}{R^3} {}_2F_1\left(2, 2+w; 3+w; -\frac{G_0\rho}{R^3}\right), \\ \gamma(R) &= \frac{9\rho^2}{R^6} {}_2F_1\left(3, 3+w; 4+w; -\frac{G_0\rho}{R^3}\right), \end{aligned} \quad (124)$$

at large distances,  $R^3 \gg G_0\rho$ , the functions (124) tend to  $\alpha(R) \simeq 1$  and  $\beta(R) \simeq \gamma(R) \simeq 0$ , for which the equation (123) reduces to  $w(R) \simeq w$ .

## V. CONCLUSIONS

In this study, we have investigated the gravitational collapse of a spherically symmetric star within the framework of AS gravity, taking into account a running gravitational coupling and a dynamical cosmological constant. The resulting equations, (29) and (30), established a general framework that can be applied to a broad class of systems with different equations of state. Our findings indicate that AS gravity changes the mechanisms of BH formation compared to classical general relativity. This introduces novel possibilities that may contribute to resolving the longstanding issue of singularities. We have demonstrated that for negative values of the equation of state parameter ( $w < 0$ ), the spherically symmetric spacetimes remain regular at the centers of BHs. For the two negative cases,  $w = -1/2$  and  $w = -1$ , we derived the field equations for both the interior and the surface of the star, as presented in Eq. (74) and Eq. (77). The spherically symmetric solutions corresponding to these equations of state have been presented in Eq. (107) and Eq. (109). Both of these spacetimes remain regular at the center of the BHs. For the cases  $w = 1/2$  and  $w = 1$ , we obtained the field equations governing both the star's interior and its surface, as detailed in Eq. (75) and Eq. (76). The corresponding spherically symmetric solutions for these equations of state are provided in

Eq. (113) and Eq. (117). These metrics possess a singularity at the center of the system. Therefore, our analysis confirms that for positive values of  $w > 0$ , the spacetime develops a central singularity. Indeed, one of the most intriguing outcomes of our work is that the final fate of a collapsing star depends strongly on EOS of the matter inside it. While traditional general relativity predicts that gravitational collapse inevitably leads to a singularity, an infinitely dense point where physics breaks down, our results indicate that under certain conditions, AS gravity can prevent this from happening. Moreover, the dynamical stability of these solutions has also been studied. It has been shown that for the values  $w = -1/2$  and  $w = 1$  the potential function given in Eq. (93) and Eq. (99) are not dynamically stable. But for the values  $w = 1/2$  and  $w = 0$  the potential functions Eq. (96) and Eq. (87) are dynamically stable.

For future research, several intriguing directions can be explored. The shadow properties of these newly proposed BHs, their thermodynamic behavior, and their quasinormal modes warrant detailed investigation. Additionally, extending the analysis to rotating solutions and examining various other aspects of BH physics could provide deeper insights into their fundamental nature. Beyond their theoretical implications, our work raises important questions about observational tests. The modifications to BH formation in AS gravity could, in principle, leave detectable imprints on astrophysical phenomena. For instance, deviations from classical collapse scenarios might be reflected in gravitational wave signals emitted by dying stars. Studying such signals in future gravitational wave observations could offer a way to test the predictions of AS gravity. Likewise, exploring its effects on BH thermodynamics and Hawking radiation could provide new insights into the nature of quantum gravity. Looking ahead, there are many exciting directions for further research. Extending our analysis to include more complex matter configurations, such as anisotropic fluids or additional fields, would help us better understand the full range of possible BH solutions in AS gravity. Additionally, investigating the stability of these solutions under small perturbations would be essential for assessing their physical viability.

In summary, our results suggest that AS gravity offers a promising alternative to classical general relativity when it comes to understanding BH formation and the nature of spacetime at extreme scales. By naturally incorporating quantum effects, this framework moves us closer to a more complete theory of gravity—one that not only respects the successes of general relativity but also addresses its most fundamental shortcomings. Continued work in this area will help us refine our understanding of BHs and, ultimately, the deep structure of the universe itself.

## ACKNOWLEDGEMENT

The work of KB was supported by the JSPS KAKENHI Grant Numbers 21K03547, 24KF0100. F.Shojai is grateful to the University of Tehran for supporting this work under a grant provided by the university research council.

### Appendix A: The hypergeometric function

The hypergeometric function  ${}_pF_q$  is defined in Ref. [104] as follows for  $a_1, \dots, a_p, b_1, \dots, b_q, z \in \mathbb{C}$

$${}_pF_q(a_1, \dots, a_p; b_1, \dots, b_q; z) = \sum_{n=0}^{\infty} \frac{(a_1)_n \dots (a_p)_n z^n}{(b_1)_n \dots (b_q)_n n!}, \quad (\text{A1})$$

where, for some parameter  $\mu$ , the Pochhammer symbol  $(\mu)_n$  is defined as

$$(\mu)_0 = 1, \quad (\mu)_n = \mu(\mu+1)\dots(\mu+n-1), \quad n = 1, 2, \dots \quad (\text{A2})$$

Another definition is that, for  $c > b > 0$  the hypergeometric function is given by the Euler integral [105],

$${}_2F_1(a, b, c; z) = \frac{\Gamma(c)}{\Gamma(b)\Gamma(c-b)} \int_0^1 t^{b-1} (1-t)^{c-b-1} (1-zt)^{-a} dt, \quad (\text{A3})$$

Moreover, the  $n$ -th derivative is given by

$$\frac{d^n}{dz^n} [{}_pF_q(a_1, \dots, a_p; b_1, \dots, b_q; z)] = \frac{(a_1)_n \dots (a_p)_n}{(b_1)_n \dots (b_p)_n} \times {}_pF_q(a_1 + n, \dots, a_p + n; b_1 + n, \dots, b_q + n; z). \quad (\text{A4})$$

Importantly, in a specific case  $(p, q) = (2, 1)$ , which is called the *Gauss hypergeometric function*, the hypergeometric function is defined for  $|z| < 1$  by the power series

$${}_2F_1(a, b, c; z) = \sum_{n=0}^{\infty} \frac{(a)_n (b)_n z^n}{(c)_n n!}, \quad z \in \mathbb{C} \quad (\text{A5})$$

$$= 1 + \frac{ab}{c} \frac{z}{1!} + \frac{a(a+1)b(b+1)}{c(c+1)} \frac{z^2}{2} + \dots \quad (\text{A6})$$

and the first order time derivative is written as

$$\frac{d}{dz} {}_2F_1(a, b, c; z) = \frac{ab}{c} {}_2F_1(a+1, b+1, c+1; z). \quad (\text{A7})$$

Apart from that, there are some useful functions for hypergeometric function which in this paper we used them frequently, the first one is written as

$${}_2F_1(1, w; w; z) = \sum_{n=0}^{\infty} \frac{(1)_n z^n}{n!}, \quad (\text{A8})$$

since  $(1)_n = n!$ , we obtain

$${}_2F_1(1, w; w; z) = \sum_{n=0}^{\infty} z^n = \frac{1}{1-z}, \quad \text{for } |z| < 1. \quad (\text{A9})$$

We now focus on the case where  $a = 1, b = 1$ , and  $c = 2$ . By substituting these values, we obtain

$${}_2F_1(1, 1; 2; -z) = \sum_{n=0}^{\infty} \frac{(1)_n (1)_n (-z)^n}{(2)_n n!} = \sum_{n=0}^{\infty} \frac{(-z)^n}{n+1},$$

Let  $n+1 = m \implies n = m-1$ . When  $n = 0, m = 1$ , the series becomes

$${}_2F_1(1, 1; 2; -z) = -\frac{1}{z} \sum_{m=1}^{\infty} \frac{(-z)^m}{m},$$

using the Taylor expansion of  $\ln(1+z)$

$$\ln(1+z) = -\sum_{m=1}^{\infty} \frac{(-z)^m}{m},$$

Therefore, for  $a = 1, b = 1, c = 2$ , the equation (A5) is written as

$${}_2F_1(1, 1; 2; -z) = \frac{\ln(1+z)}{z}. \quad (\text{A10})$$

We now substitute the values  $a = 1, b = \frac{1}{2}$ , and  $c = \frac{3}{2}$  into the series Eq. (A5)

$${}_2F_1\left(1, \frac{1}{2}; \frac{3}{2}; -z\right) = \sum_{n=0}^{\infty} \frac{(1)_n \left(\frac{1}{2}\right)_n (-z)^n}{\left(\frac{3}{2}\right)_n n!} = \sum_{n=0}^{\infty} \frac{(-z)^n}{2n+1},$$

using the series

$$\arctan(\sqrt{z}) = \sum_{n=0}^{\infty} (-1)^n \frac{z^{n+1/2}}{2n+1},$$

one can simplify the calculations. Therefore, in the case  $a = 1, b = \frac{1}{2}, c = \frac{3}{2}$  the Gauss hypergeometric function is written as

$${}_2F_1\left(1, \frac{1}{2}; \frac{3}{2}; -z\right) = \frac{\arctan \sqrt{z}}{\sqrt{z}}. \quad (\text{A11})$$

We have another function for the case  $a = 1, b = 2, c = 3$  which is given as

$${}_2F_1(1, 2; 3; -z) = \sum_{n=0}^{\infty} \frac{(1)_n (2)_n (-z)^n}{(3)_n n!}, \quad (\text{A12})$$

where

$$\frac{(1)_n (2)_n}{n! (3)_n} = \frac{2}{n+2}, \quad (\text{A13})$$

inserting this equation into Eq. (A12) tends to the following equation

$${}_2F_1(1, 2; 3; -z) = \frac{2}{z^2} \sum_{n=2}^{\infty} \frac{(-z)^n}{n}, \quad (\text{A14})$$

this series resembles the Taylor series for the natural logarithm. We recall that

$$-\ln(1+z) = \sum_{n=1}^{\infty} \frac{(-z)^n}{n} \quad \text{for } |z| < 1,$$

to relate it to our series, we can write

$$\sum_{n=2}^{\infty} \frac{(-z)^n}{n} = -\ln(1+z) + z, \quad (\text{A15})$$

which is valid for  $|z| < 1$ . Substituting Eq. (A15) into Eq. (A12) becomes

$${}_2F_1(1, 2; 3; -z) = \frac{2}{z} - \frac{2\ln(1+z)}{z^2}. \quad (\text{A16})$$

An additional significant case discussed in this paper corresponds to  $a = 1$ ,  $b = \frac{3}{2}$ , and  $c = \frac{5}{2}$ , presented as

$${}_2F_1\left(1, \frac{3}{2}; \frac{5}{2}; -z\right) = -\frac{3}{z} \sum_{n=1}^{\infty} \frac{(-z)^n}{1+2n}, \quad (\text{A17})$$

to analyze this series, we utilize the following integral

$$\frac{1}{1+2n} = \int_0^1 x^{2n} dx, \quad (\text{A18})$$

substituting this integral into the series in Eq. (A17) leads to

$$\sum_{n=1}^{\infty} \frac{(-z)^n}{1+2n} = \int_0^1 \sum_{n=1}^{\infty} (-zx^2)^n dx = -1 + \frac{\arctan(\sqrt{z})}{\sqrt{z}}, \quad (\text{A19})$$

to derive the above equation, we employed the series  $\sum_{n=0}^{\infty} y^n = \frac{1}{1-y}$ . Substituting this series into Eq. (A17) results in

$${}_2F_1\left(1, \frac{3}{2}; \frac{5}{2}; -z\right) = \frac{3}{z} \left(1 - \frac{\arctan(\sqrt{z})}{\sqrt{z}}\right). \quad (\text{A20})$$

- 
- [1] R. Penrose, *Phys. Rev. Lett.* **14**, 57 (1965).
  - [2] J. D. Bekenstein, *Phys. Rev. D* **7**, 2333 (1973).
  - [3] J. D. Bekenstein, *Phys. Rev. D* **9**, 3292 (1974).
  - [4] J. D. Bekenstein, *Lett. Nuovo Cim.* **4**, 737 (1972).
  - [5] S. W. Hawking, *Commun. Math. Phys.* **43**, 199 (1975).
  - [6] S. W. Hawking, *Nature* **248**, 30 (1974).
  - [7] J. M. Bardeen, B. Carter, and S. W. Hawking, *Commun. Math. Phys.* **31**, 161 (1973).
  - [8] S. W. Hawking and D. N. Page, *Commun. Math. Phys.* **87**, 577 (1983).
  - [9] S. W. Hawking, *Phys. Rev. D* **14**, 2460 (1976).
  - [10] A. Almheiri, T. Hartman, J. Maldacena, E. Shaghoulian, and A. Tajdini, *Rev. Mod. Phys.* **93**, 035002 (2021).
  - [11] A. Ashtekar, J. Olmedo, and P. Singh, *Phys. Rev. D* **98**, 126003 (2018).
  - [12] A. Ashtekar, J. Baez, A. Corichi, and K. Krasnov, *Phys. Rev. Lett.* **80**, 904 (1998).
  - [13] A. Ashtekar, J. Olmedo, and P. Singh, *Phys. Rev. Lett.* **121**, 241301 (2018).
  - [14] A. Bonanno and M. Reuter, *Phys. Rev. D* **62**, 043008 (2000).
  - [15] J. R. Oppenheimer and H. Snyder, *Physical Review* **56**, 455 (1939).
  - [16] S. Datt, *Journal of Physics* **108**, 314 (1938).
  - [17] V. P. Frolov and G. A. Vilkovisky, *Phys. Lett. B* **106**, 307 (1981).
  - [18] F. Shojai, A. Sadeghi, and R. Hassannejad, *Class. Quant. Grav.* **39**, 085003 (2022).
  - [19] R. Hassannejad, G. Lambiase, F. Scardigli, and F. Shojai, *Phys. Rev. D* **111**, 064069 (2025).
  - [20] R. Hassannejad, A. Sadeghi, and F. Shojai, *Class. Quant. Grav.* **40**, 075002 (2023).
  - [21] J. Lewandowski, Y. Ma, J. Yang, and C. Zhang, *Phys. Rev. Lett.* **130**, 101501 (2023).
  - [22] A. Bonanno, B. Koch, and A. Platania, *Found. Phys.* **48**, 1393 (2018).
  - [23] Y. B. Zel'dovich and I. D. Novikov, *Sov. Astron.* **10**, 602 (1967).
  - [24] B. J. Carr and S. W. Hawking, *Mon. Not. Roy. Astron. Soc.* **168**, 399 (1974).
  - [25] S. Hawking, *Mon. Not. Roy. Astron. Soc.* **152**, 75 (1971).
  - [26] S. W. Hawking, *Communications in Mathematical Physics* **25**, 152 (1972).
  - [27] S. W. Hawking and R. Penrose, *Proc. Roy. Soc. Lond. A* **314**, 529 (1970).
  - [28] R. Penrose, *Riv. Nuovo Cim.* **1**, 252 (1969).
  - [29] S. W. Hawking, *Physical Review D* **13**, 191 (1976).
  - [30] S. W. Hawking, *Nature* **248**, 30 (1974).
  - [31] M. Bojowald, *Phys. Rev. Lett.* **95**, 061301 (2005).
  - [32] M. Reuter and A. Bonanno, *Physical Review D* **62**, 043008 (2000).
  - [33] M. Reuter, *Physical Review D* **57**, 971 (1998).
  - [34] M. Reuter and F. Saueressig, *Physical Review D* **65**, 065016 (2002).
  - [35] A. Bonanno and M. Reuter, *Physical Review D* **65**, 043508 (2001).
  - [36] J. M. Maldacena, Ph.D. thesis, Princeton U. (1996), [arXiv:hep-th/9607235](https://arxiv.org/abs/hep-th/9607235).
  - [37] S. W. Hawking and G. F. R. Ellis, (Cambridge University Press, Cambridge, 1973).
  - [38] G. 't Hooft, *Nucl. Phys. B* **256**, 727 (1985).
  - [39] C. G. Callan and J. M. Maldacena, in *ICTP Summer School in High-energy Physics and Cosmology* (1996) pp. 1–65.

- [40] J. M. Maldacena, A. Strominger, and E. Witten, *JHEP.* **12**, 002 (1997).
- [41] G. T. Horowitz and J. M. Maldacena, *JHEP.* **02**, 008 (2004).
- [42] J. Maldacena and L. Susskind, *Fortsch. Phys.* **61**, 781 (2013).
- [43] S. Weinberg, in *General Relativity: An Einstein Centenary Survey*, edited by S. W. Hawking and W. Israel (Cambridge University Press, Cambridge, 1979) pp. 790–831.
- [44] G. 't Hooft and M. J. G. Veltman, *Annales de l'Institut Henri Poincaré* **20**, 69 (1974).
- [45] A. Bonanno, A.-P. Khosravi, and F. Saueressig, *Phys. Rev. D* **107**, 024005 (2023).
- [46] D. Dou and R. Percacci, *Class. Quant. Grav.* **15**, 3449 (1998).
- [47] A. Ashtekar, *Gen. Rel. Grav.* **41**, 707 (2009).
- [48] K. Becker, M. Becker, and J. Schwarz, (Cambridge University Press, 2006).
- [49] R. Gambini and J. Pullin, 1st ed. (Oxford University Press, 2011).
- [50] A. B. Platania, Springer Theses (Springer, 2018) p. 142.
- [51] A. Codello and R. Percacci, *Phys. Rev. Lett.* **97**, 221301 (2006).
- [52] E. S. Fradkin and G. A. Vilkovisky, *Phys. Lett. B* **77**, 262 (1978).
- [53] S. Weinberg, in *General Relativity: An Einstein Centenary Survey* (1980) pp. 790–831.
- [54] D. F. Litim, *Phys. Rev. Lett.* **92**, 201301 (2004).
- [55] C. Wetterich, *Physics Letters B* **301**, 90 (1993).
- [56] M. H. Goroff and A. Sagnotti, *Nuclear Physics B* **266**, 709 (1986).
- [57] J. Polonyi, *Central Eur. J. Phys.* **1**, 1 (2003).
- [58] P. F. Machado and F. Saueressig, *Phys. Rev. D* **77**, 124045 (2008).
- [59] O. Lauscher and M. Reuter, *Phys. Rev. D* **66**, 025026 (2002).
- [60] M. Reuter and F. Saueressig, *Phys. Rev. D* **65**, 065016 (2002).
- [61] O. Lauscher and M. Reuter, *Phys. Rev. D* **65**, 025013 (2002).
- [62] W. Souma, *Prog. Theor. Phys.* **102**, 181 (1999).
- [63] B. Knorr and F. Saueressig, *Phys. Rev. Lett.* **121**, 161304 (2018).
- [64] A. Bonanno, D. Malafarina, and A. Panassiti, *Phys. Rev. Lett.* **132**, 031401 (2024).
- [65] L. Bosma, B. Knorr, and F. Saueressig, *Phys. Rev. Lett.* **123**, 101301 (2019).
- [66] A. Platania, *Eur. Phys. J. C* **79**, 470 (2019).
- [67] A. Platania, *Gen. Rel. Grav.* **57**, 58 (2025).
- [68] A. Bonanno and M. Reuter, *Phys. Rev. D* **65**, 043508 (2002).
- [69] M. Reuter and F. Saueressig, *JCAP.* **09**, 012 (2005).
- [70] B. Koch and I. Ramirez, *Class. Quant. Grav.* **28**, 055008 (2011).
- [71] A. Bonanno and M. Reuter, *JCAP.* **08**, 024 (2007).
- [72] A. Bonanno and S. Carloni, *New J. Phys.* **14**, 025008 (2012).
- [73] S. Weinberg, *Phys. Rev. D* **81**, 083535 (2010).
- [74] A. Bonanno and A. Platania, *Phys. Lett. B* **750**, 638 (2015).
- [75] L.-H. Liu, T. Prokopec, and A. A. Starobinsky, *Phys. Rev. D* **98**, 043505 (2018).
- [76] A. Silva, *Phys. Lett. B* **860**, 139154 (2025).
- [77] A. Platania, *Universe* **5**, 189 (2019).
- [78] G. Kofinas and V. Zariwas, *Phys. Rev. D* **94**, 103514 (2016).
- [79] N. Christiansen, D. F. Litim, J. M. Pawłowski, and M. Reichert, *Phys. Rev. D* **97**, 106012 (2018).
- [80] P. Donà, A. Eichhorn, P. Labus, and R. Percacci, *Phys. Rev. D* **93**, 044049 (2016).
- [81] J. Meibohm, J. M. Pawłowski, and M. Reichert, *Phys. Rev. D* **93**, 084035 (2016).
- [82] P. Donà, A. Eichhorn, and R. Percacci, *Phys. Rev. D* **89**, 084035 (2014).
- [83] G. P. Vacca and O. Zanusso, *Phys. Rev. Lett.* **105**, 231601 (2010).
- [84] C. Laporte, A. D. Pereira, F. Saueressig, and J. Wang, *JHEP* **12**, 001.
- [85] R. R. Caldwell, M. Kamionkowski, and N. N. Weinberg, *Phys. Rev. Lett.* **91**, 071301 (2003).
- [86] R. R. Caldwell, *Phys. Lett. B* **545**, 23 (2002).
- [87] V. V. Kiselev, *Class. Quant. Grav.* **20**, 1187 (2003).
- [88] S. Weinberg, *Cosmology* (Oxford University Press, 2008).
- [89] S. M. Carroll, M. Hoffman, and M. Trodden, *Phys. Rev. D* **68**, 023509 (2003).
- [90] M. A. Markov and V. F. Mukhanov, *Nuovo Cim. B* **86**, 97 (1985).
- [91] V. Fock, 2nd ed. (Pergamon Press, Oxford, UK, 1959).
- [92] A. Einstein, *Annalen Phys.* **49**, 769 (1916).
- [93] W. Israel, *Nuovo Cim. B* **44S10**, 1 (1966).
- [94] A. Bonanno and F. Saueressig, *Comptes Rendus Physique* **18**, 254 (2017).
- [95] T. Harada, C.-M. Chen, and R. Mandal, (2025), [arXiv:2502.16787 \[gr-qc\]](https://arxiv.org/abs/2502.16787).
- [96] P. O. Mazur and E. Mottola, *Proc. Nat. Acad. Sci.* **101**, 9545 (2004).
- [97] D. Glavan and C. Lin, *Phys. Rev. Lett.* **124**, 081301 (2020).
- [98] P. G. S. Fernandes, P. Carrilho, T. Clifton, and D. J. Mulryne, *Class. Quant. Grav.* **39**, 063001 (2022).
- [99] J. G. Kelly, R. Santacruz, and E. Wilson-Ewing, *Phys. Rev. D* **102**, 106024 (2020).
- [100] R. Gambini, J. Olmedo, and J. Pullin, *Class. Quant. Grav.* **37**, 205012 (2020).
- [101] J. Abedi and H. Arfaei, *JHEP* **03**, 135.
- [102] M. Visser, *Class. Quant. Grav.* **37**, 045001 (2020).
- [103] R. Saadati and F. Shojai, *Class. Quant. Grav.* **38**, 135025 (2021).
- [104] W. Koepf, 2nd ed., Universitext (Springer, London, 2014).
- [105] G. Heckman, Tsinghua lectures on hypergeometric functions (2015), december 8, 2015, [G.Heckman@math.ru.nl](mailto:G.Heckman@math.ru.nl).
- [106] J. Lewandowski, Y. Ma, J. Yang, and C. Zhang, *Phys. Rev. Lett.* **130**, 101501 (2023).